# Electron transfer in liquid–solid contact electrification and double-layer formation

**Shiquan Lin**[a,b,*], **Xiangyu Chen**[a,b,*], **and Zhong Lin Wang**[a,c,*], [a] Beijing Institute of Nanoenergy and Nanosystems, Chinese Academy of Sciences, Beijing, P. R. China; [b] School of Nanoscience and Technology, University of Chinese Academy of Sciences, Beijing, P. R. China; and [c] School of Materials Science and Engineering, Georgia Institute of Technology, Atlanta, GA, United States





## Key points

This chapter provides a summary about recent studies on the charge transfer at liquid–solid CE. Besides ion transfer at the interface that is set for decades, electron transfer is found to play a dominant role in some cases.

- A series of experiments with different observation techniques in both microscale and large scale have been systematical introduced to clarify the mechanism of electron transfer at liquid–solid interface.
- Based on existing studies, the formation of electric double-layer (EDL) is revisited owing to the contribution from electron transfer in liquid–solid CE, and a hybrid EDL model with a two-step formation process is proposed, in which both electron transfer and ion adsorption are taken into consideration.
- The applications of CE at liquid–solid interface using the TENG as an energy harvester, sensor, chemical reactor and so on, are systematically summarized.
- The impacts of electron transfer and the hybrid EDL model on the applications of electrochemistry storage, interfacial reaction, EDL electronics and many other research fields that relate to liquid–solid charge transfer are further discussed.

## Abstract

The liquid–solid (L-S) interface is one of the most important surface sciences subject in chemistry, catalysis, energy provision and even biology. The formation of an electric double-layer (EDL) at the L-S interface is thought to be due to the adsorption of a layer of ions on the solid surface, resulting in the redistribution of ions in the liquid. Although the existence of a layer of charge on a solid surface has always been assumed, the source of the charge has not been widely explored. Recent studies of contact electrochemistry (CE) between liquids and solids have shown that electron transfer plays a dominant role in the initial stage of charge layer formation at the L-S interface. Here, we review recent studies on electron transfer in liquid–solid CE, including liquid-insulator, liquid-semiconductor, and liquid-metal scenarios. Considering the existence of electron transfer on the L-S interface, we reconsider the formation of EDL. In addition, a liquid–solid CE based triboelectric nanogenerator (TENG) technique is introduced, which can be used not only to obtain mechanical energy from liquid, but also as a probe to detect charge transfer at liquid–solid interface.

[*]These authors contributed equally to this review.

## Introduction

CE (contact electrification) is the scientific term of triboelectrification, which is a conjunction of fractioning and CE. The nature of transferred charges in CE for solid materials have been debated for decades being electrons,[1–4] ions[5–8] and even materials species,[9–11] without a conclusive result. Recently, charge transfer at solid–solid CE is determined to be dominated by electron transfer by using Kelvin probe force microscopy (KPFM) and thin-film studying using triboelectric nanogenerator (TENG).[12–14] Related physics models have been proposed for cases such as dielectric–dielectric and metal–dielectric interfaces. CE can occur at almost all solid–solid,[15–19] liquid–solid[20–23] and liquid–liquid[24–26] interfaces, and may also occur at solid–gas and liquid–gas interfaces (**Fig. 1**).

Charge transfer at liquid–solid interface is a topic of broad interest in chemistry, especially in electrochemistry,[27–32] catalysis[33–37] *etc*. Many physical and biological phenomena are also related to charge transfer at the liquid–solid interface, such as electrowetting,[38–41] colloidal suspension,[42–45] photovoltaic effect,[46–49] photosynthesis[50–52] *etc*. The fundamental sciences related to studies in above fields have been developed for decades, but are mainly focused on some specific liquid–solid interface systems, such as $TiO_2$-water interface, which is one of the key topics in water splitting.[53–55] On the contrary, liquid–solid CE concerns almost all liquid–solid interfaces. Therefore, it is of general significance to understand the charge transfer at liquid–solid interface from the view of liquid–solid CE. When it comes to the liquid–solid CE, there are two basic issues. A core problem in liquid–solid CE is the identity of the charge carriers, and the other is the formation of the EDL.[56] In the studies about electrochemistry,[57,58] catalysis[59] and colloidal suspension,[60,61] the identity of the charge carriers and formation of the EDL are important. It was suggested that the charge transfer at liquid–solid interface may be due to adsorption of ions from the liquid on the solid surface,[62,63] or the electron transfer from liquid side to the solid side, which is accompanied by chemical reactions.[64–66] Electron transfer is generally considered when the solid is a conductor or semiconductor. And the adsorption of ions is traditionally considered to be responsible for the generation of charge transfer at the liquid–solid interface when the solid is an insulator. For the EDL, traditional studies focused on the distribution of ions and the structure of water molecules on the liquid side,[67–69] and the fundamental study of the identity of the charge carriers on the solid surface of the EDL is a forgotten corner in general chemistry.

In the history of CE research, most studies focused on the solid–solid condition, and did not pay attention to liquid–solid CE.[70–75] Therefore, the mechanism of liquid–solid coupling is more mysterious than that of solid coupling. In the 1980s, CE between liquid metal and solid insulator was studied, which was one of the early works on liquid–solid CE.[76] In the 1990s, Matsui and Yatsuzuka et al. studied the electrochemical phenomenon between water droplets and the surface of an insulator.[77–79] Studies have shown that water droplets are always positively charged when they slide over surfaces of insulators such as PTFE and resins. In addition, Burgo et al. quantified the position of water in the three-power series in 2016.[80] In the above work, the adsorption of water to anions on the surface of the insulator is considered to be the cause of contact charging between water and the insulator. In fact, once water is involved in CE, even in solid–solid CE, ion transfer is always assumed to be responsible for CE,[6,81,82] but there is no solid evidence.

Unlike solid-state CE, the identity of charge carriers in liquid–solid CE is assumed to be ions due to solution involvement, but this basic assumption in liquid–solid CE has not even been experimentally verified. However, due to the invention of liquid–solid nanogenerators (L-S TENGs), detailed studies have recently been carried out.[83–94] L-S TENGs were developed based on the conversion of mechanical energy into electrical energy by the charge effect on liquid and solids, rekindling researchers' interest in charge on liquid and solids. Recently, the properties of charge carriers in liquid–solid CE have been re-examined.[95–97] Liquid-solid CE has been studied at the nanoscale and macro scale. Data show that both electron and ion transfer occur in liquid–solid CE, and electron transfer may even play a dominant role in some cases. The key to distinguishing the transferred charge from that of an ion or electron can be accomplished by two methods: temperature-induced electron thermionic emission[13,98]; And UV-induced electron

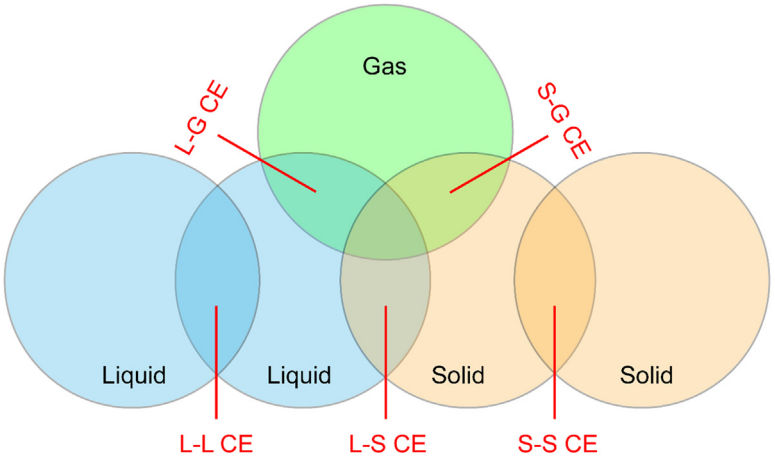


**Fig. 1** Schematic of the contact electrification between different phases. CE can occur at almost all solid–solid, liquid–solid and liquid–liquid interfaces, and may also at solid–gas and liquid–gas interfaces.

emission,[14] simply because neither method can release adsorbed ions on the surface if the temperature is moderate. In experiments, we found that the charge on the solid surface generated by liquid–solid CE can be emitted by thermal excitation, which means that electron transfer does exist in liquid–solid CE.[95] It has been calculated that the number of ions in deionized water (DI water) is insufficient to produce the observed charge density in liquid–solid CE.[96] Based on electron transfer in liquid–solid CE, Wang et al. first proposed a "two-step" model for EDL formation, in which electron transfer plays a leading role in the first step.[56]

In summary, liquid–solid CE was not sufficiently discussed in early studies, and the charge carrier in liquid–solid CE was considered to be ion, and electron transfer was not even considered. The mechanism of liquid–solid CE has recently been re-examined due to the invention of L-S TENG. It has been proposed that electron transfer exists in liquid–solid CE. In addition, a "two-step" model has been proposed in which electron transfer between liquid molecules and solid surface atoms is the first step, followed by ion transfer due to electron interactions.[56] The two-step model provides a new way to understand the formation of EDL, which could have major implications for basic chemistry and even biology.

## The typical electric double-layer model

The EDL model is often used to describe the charges and potential distribution at the liquid–solid interface, which is a core topic in electrochemistry. Helmholtz[99] was the first to propose the notion of EDL, discovering that at the electrode/electrolyte interface, two layers of opposite charges formed with minimal space. The conception was then revised by Gouy and Chapman,[100,101] who suggested that the ions are spread in a thin layer region rather than being tightly bonded on the solid surface. Stern[102] integrated the Helmholtz and Gouy–Chapman models in 1924 and proposed the concept of two distinct charge regions: the Stern layer and the diffuse layer, as depicted in Fig. 2A. The Stern layer (SL) is comprised of the ions (usually hydrated) firmly adsorbed on the charged electrode, and the diffuse layer (DL) is relevant to the density of ions (with opposite polarity to that of the electrode), which diminishes with distance away from the surface. The Gouy–Chapman–Stern EDL model has been broadly taken on in many fields, covering electrolyte capacitor,[103] electrochemistry reaction,[104] capacitive deionization,[105,106] electric twofold layer transistor,[107] and electrowetting.[108,109] As is shown in Fig. 2A, the EDL is triggered by an external field applied to the electrode, and the EDL formation on the surface of pre-charged insulators is comparable to that on the electrode with the applied field. Meanwhile, when entering the double layer, the ions with weaker solvation shells usually give away part of their solvation shells and only some solvated ions with a strong solvation shell (such as fluoride) can be held in position by purely electrostatic forces (Fig. 2A). According to traditional EDL theory,[109] the chemical interaction between half-solvated anions and the electrode surface can produce additional charges on the electrode, followed by the countercharge being attracted to the bilayer for charge compensation. In addition, the EDL can also be formed in this case for solid materials with abundant chemical groups by ionization or dissociation reactions between the solid surface and the liquid. An example is shown in Fig. 2B, carbon materials with carboxyl groups (-COOH) can attract counterions decorated with ionization-rich groups (e.g., -COO-). Such EDL pictures are commonly used in colloidal science,[110] cell biology, and capacitive mixing.[111,112]

## Contact electrification at liquid–solid interface

### Liquid-dielectric contact electrification

The decay of three charges on the surface of an insulator caused by thermionic emission has proved to be a method for differentiating electron and ion transfer in solid–solid CE.[13,98] Based on thermionic emission theory, Lin et al. designed a nanoscale charge decay experiment using Kelvin probe force microscopy (KPFM) to quantify electron and ion transfer between aqueous solution and

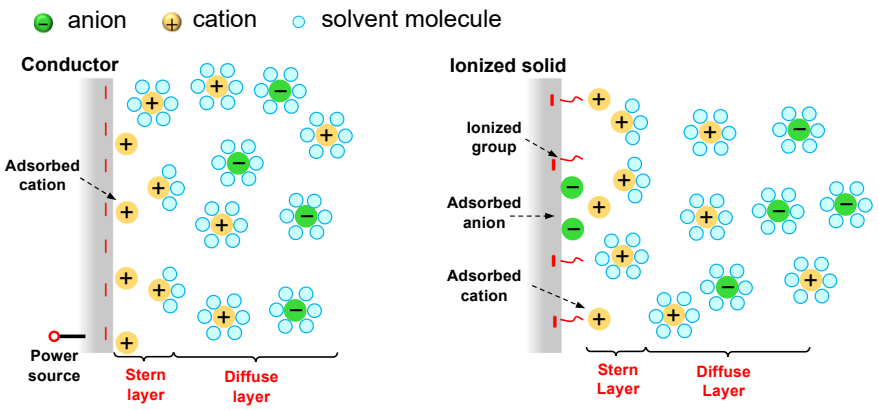


**Fig. 2** Typical EDL model. (A) EDL on the electrode surface (B) EDL on the ionized solid surface. The ion distribution near the surface can be divided into stern layer and diffuse layer.

insulator.[95] In the experiment, the initial surface charge density of the insulator sample, such as $SiO_2$, $Si_3N_4$, MgO, was measured by using KPFM. The water-based droplets then slide over the surface of the insulator, in the process transferring electric charge from the liquid to the surface of the insulator. As shown in Fig. 3A, the charge on the surface of the insulator generated in liquid–solid CE may be electrons or ions. Ions are produced by ionization reactions on oxide and nitride surfaces.[113–117] After CE, the insulator sample is heated to a certain temperature (e.g., 513 K), and according to the thermionic emission theory in CE, electrons will be thermically excited and emitted from the insulator surface, as shown in Fig. 3B. But in the case of ions, they form covalent bonds with atoms on the surface of the insulator, which is equivalent to chemisorption rather than physical adsorption. For chemisorption of ions on solid surfaces, such as $OH^-$ and $H^+$ on $SiO_2$ surface, the energy threshold of $OH^-$ removal from $SiO_2$ surface is about 8.5 eV,[118] while the energy threshold of $H^+$ removal is about 20 eV.[119] Therefore, the chemical ions adsorbed on the surface are quite difficult to remove from the surface at moderate temperatures.

Fig. 3C shows the results of the charging and heating cycle tests. $SiO_2$'s initial surface charge density is close to zero. When it comes into contact with deionized water, the negative charge is transferred from the deionized water to the $SiO_2$ surface. During the heating process (at 513 K and held for 10 min), the surface charge density decreases due to electron thermorelease. In the first cycle, we note that some charges cannot be removed from the surface ("sticky" charges), which can be identified as the ions produced at the surface in liquid–solid CE. As the flow circulates, the density of the "sticky" charge increases, eventually reaching saturation. This is because the available charge positions on the surface of an insulator are limited given the breakdown field. When an ion is attached to a surface, an available charge location is permanently occupied. In the next cycle of contact charging with deionized water, both electrons and ions are transferred to the surface, but the number of transferred electrons is reduced by the number of available charge locations. Therefore, the movable charge on the insulator surface decreases as the test period increases. Although ions accumulate on the surface, electron transfer dominates the CE between the original $SiO_2$ surface and the deionized water on first contact, with a ratio of more than 3.4.

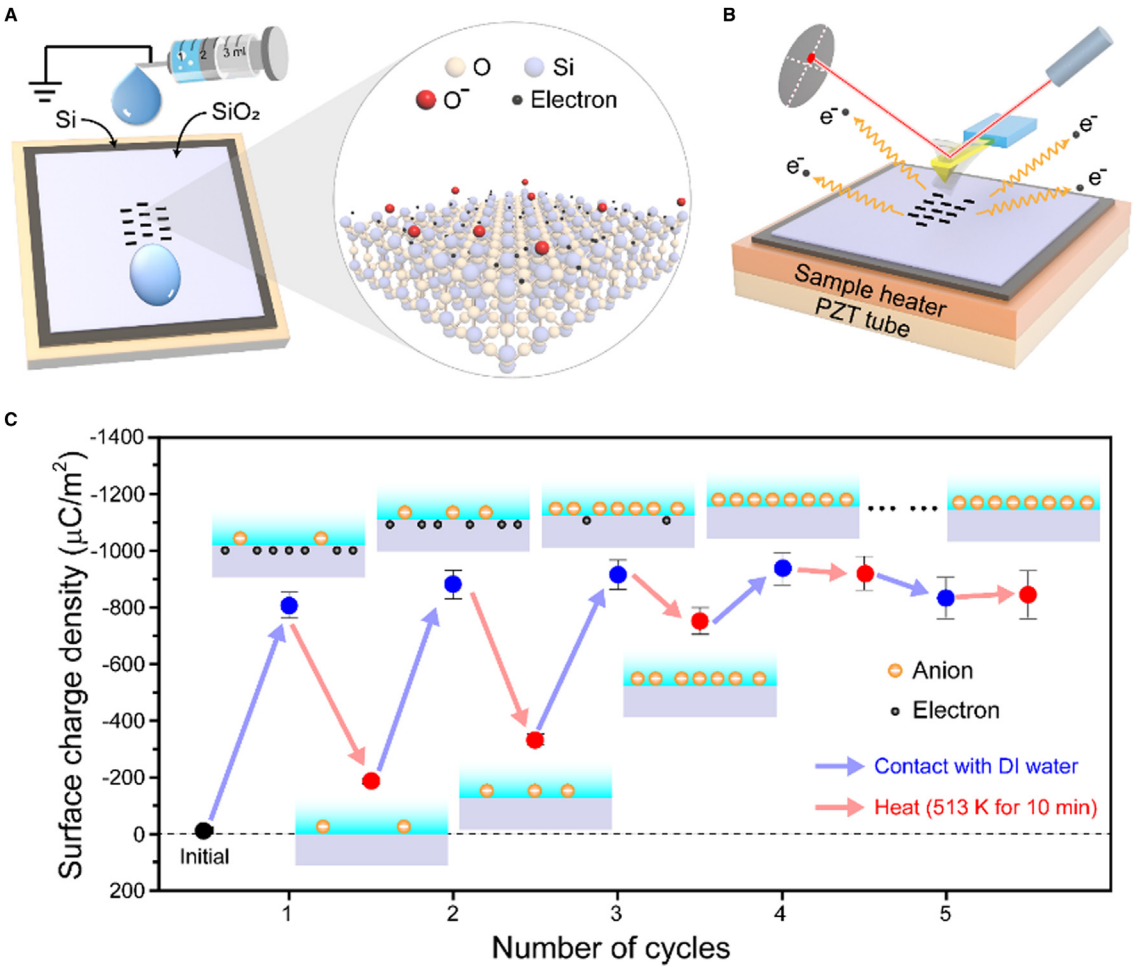


**Fig. 3** Temperature effect on the contact electrification between DI water and $SiO_2$.[95] (A) The setup of the contact charge experiment. (B) The setup of AFM platform for the thermionic emission experiments. (C) The charge density on the $SiO_2$ surface in the charging and heating cycle tests. Reproduced with permission from Ref. 95, Copyright 2020 Nature spring.

Fig. 4 shows the effect of temperature on CE between DI water and different insulators. It is found that the charge density on the surface of the insulator decays exponentially, which is consistent with thermionic emission theory. For some materials, the surface charge density becomes corrected, which means that the solid receives electrons in CE (Fig. 4A and C). Some solids accept holes, such as $Si_3N_4$, $HfO_2$, $Al_2O_3$ and AlN. It is easy to understand that at high temperatures the negative charge density ($SiO_2$) or positive charge density ($Si_3N_4$, $HfO_2$) decreases over time. This is because the negative charges on a solid surface are electrons and negative ions, while the positive charges are holes and positive ions. Electrons and holes are emitted at high temperatures, causing a decay in the surface charge density. Surprisingly, the charge density on some materials, such as magnesium oxide and $Al_2O_3$, increases with decay time, meaning that solids in contact with deionized water can receive both electrons and positive ions (magnesium oxide), or both holes and negative ions ($Al_2O_3$). These results imply that electron and ion transfer are independent of each other in liquid–solid CE. In addition, electrons and ions produced in liquid–solid CE may be isolated in different surface regions.

In addition to KPFM, many other experimental methods have been applied to study CE at the liquid–solid interface, and TENG is one of the powerful techniques in this regard. Nie et al. designed an extruding system to elucidate the electrochemical properties between liquids and solids. Polytetrafluorethylene (PTFE) membranes are used as solids because they are fairly stable to acid or base solutions.[96] The droplets are positioned between two FTO-PTFE substrates, and the extrusion motion of the substrate is precisely controlled by a linear motor. The detailed extrusion process of DI water droplets is shown in Fig. 5A. The water distributed evenly and finally turned into a thin liquid film, resulting in a large contact area between the liquid and PTFE film. After the contact separation process, an electric meter can be used to measure the amount of charge on the DI droplet (50 μL), as shown in Fig. 5B. As the contact area increases, so does the amount of induced charge on the droplet. To determine the contribution of electron transfer and ion adsorption, simple calculations were performed according to the pure ion adsorption model, also seen in Fig. 5B. At the liquid–solid interface, the ionic diffusion thickness is estimated to be ~20 nm. In general, this diffusion region of hydroxide ions is usually from a few angstroms to tens of angstroms.[120,121] In addition, the contact period between PTFE and droplets is controlled to be less than 2 s, which is insufficient for the diffusion of free ions in deeper regions. Ideally, a value of 20 nm is an ideal value that

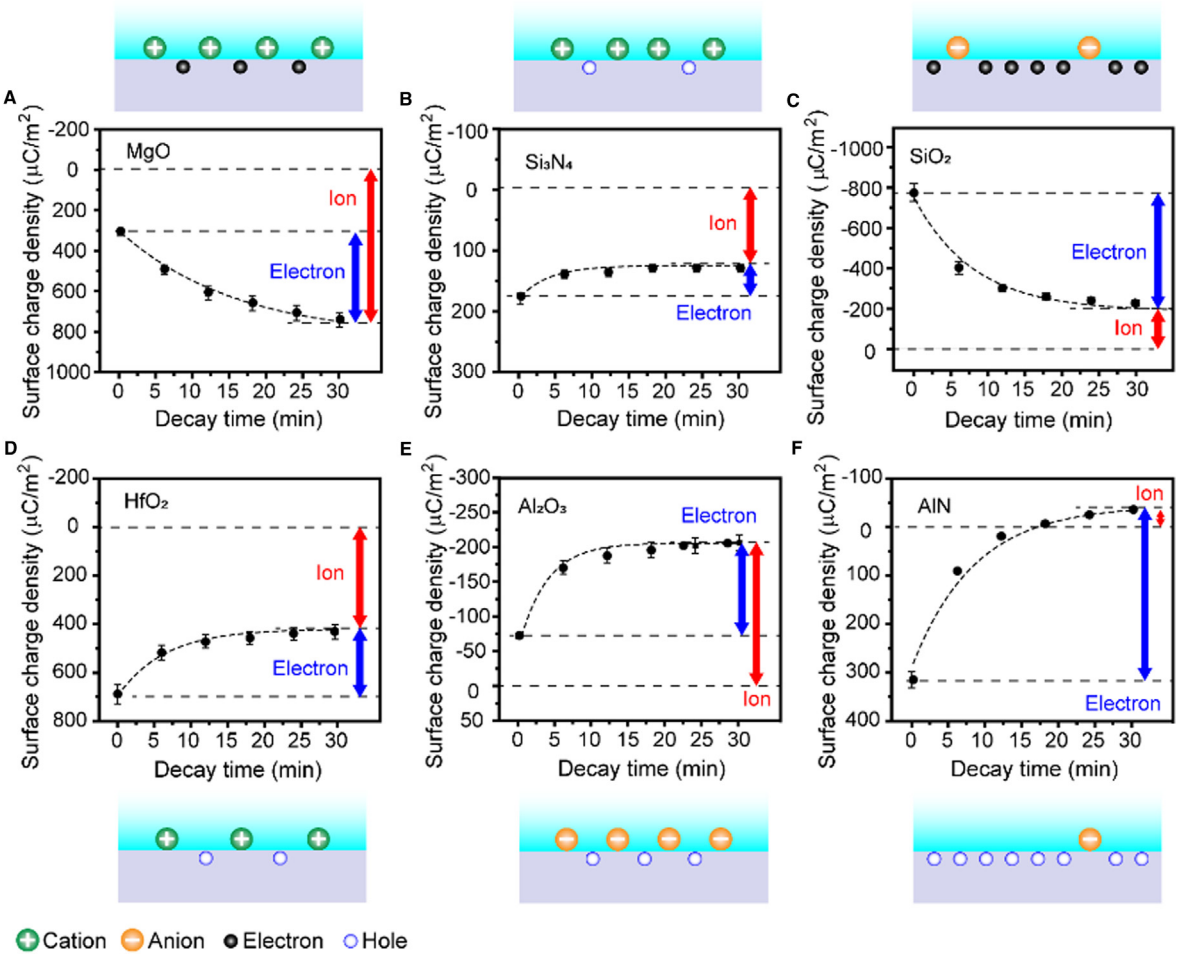


**Fig. 4** Temperature effect on the contact electrification between DI water and different insulator surfaces.[95] (A) MgO, (B) $Si_3N_4$, (C) $SiO_2$, (D) $HfO_2$, (E) $Al_2O_3$ and (F) AlN. As for ion adsorption, both physical adsorption and chemical adsorption are possible, and they can be quantified using the method introduced by *Lin* et al. Reproduced with permission from Ref. 95, Copyright 2020 Nature spring.

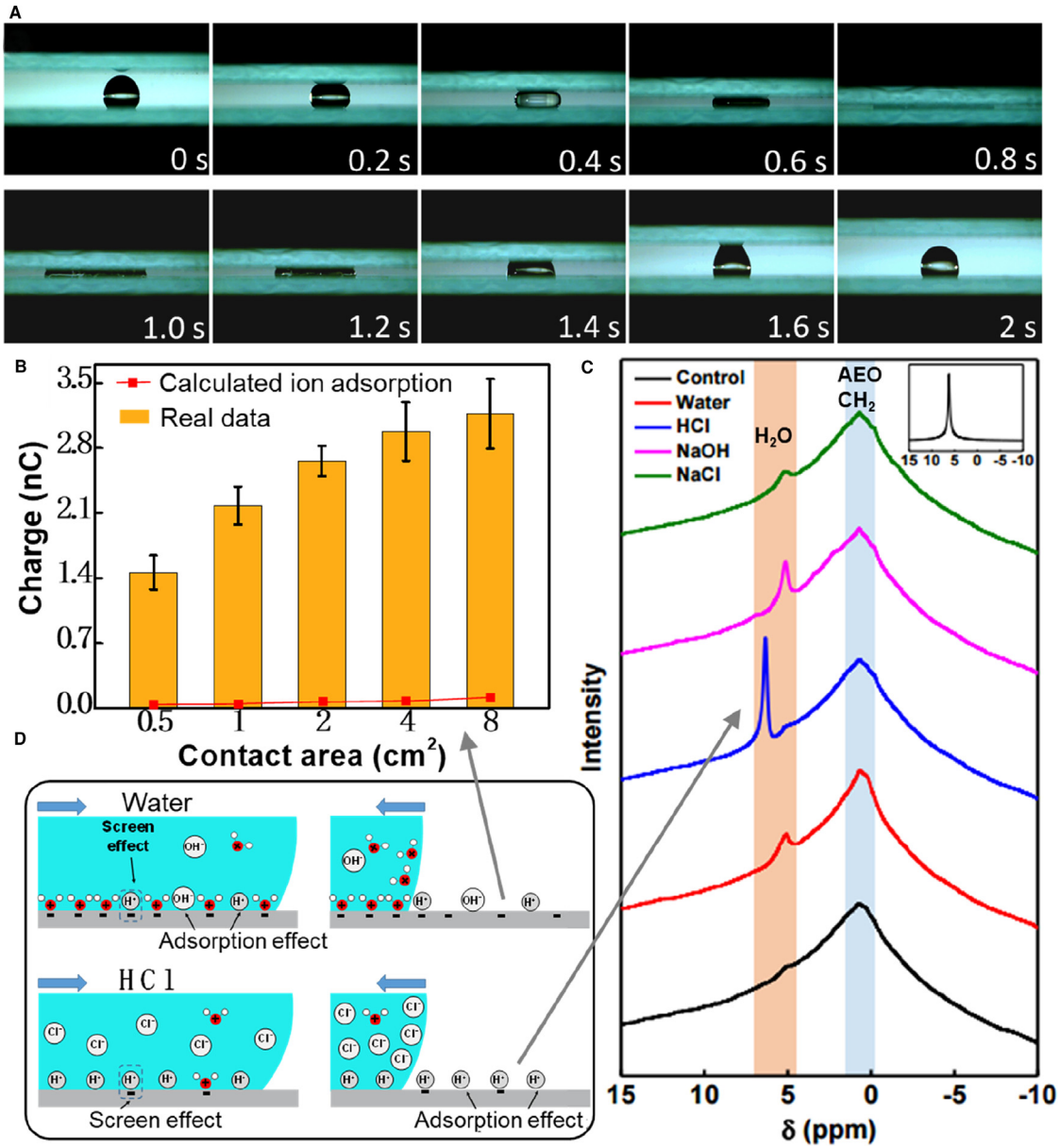


**Fig. 5** A squeezing system for studying the liquid–solid contact electrification.[96] (A) squeezing-recovering process of a droplet, (B) The amount of charges on deionized water (50 μL) after contacting with PTFE membrane and the theoretically calculation based on ion transfer model. Here, the experimental result is 10 times larger than calculated value. (C) 1H nuclear magnetic resonance spectrum of PTFE. Insert: 1H NMR spectrum of HCL solution (5 mol $L^{-1}$). (D) CE induced charge generation between water (HCl) and PTFE film. Reproduced with permission from Ref. 96. Copyright 2020 Wiley.

maximizes the likelihood of ion adsorption. Many inhibitory factors, such as the inhibitory effect of hydrogen ions ($H^+$), were ignored in the calculations. A comparison of experimental and computational results in Fig. 5B suggests that the ion transfer process may provide as little as 10% of the total charge. Therefore, the electron transfer process must be considered in the CE process between water and PTFE.

In order to verify the possible ion adsorption on PTFE surface, a solid state 1H nuclear magnetic resonance (NMR) spectrometer was used to measure the change of element H after CE, as shown in Fig. 5C. In all five spectra, the same peak signal appeared at the same location (about 0.7 PPM), which was related to the primary alcohol ethoxylates (AEO, RO (CH2CH2O) nH) in the PTFE dispersion. The 1H signal of water appears around 4.8 PPM.[122] After contact with deionized water, NaCl solution and NaOH solution, the 1H NMR signal has a similar peak value. However, the amount of charge transfer after contact with deionized water is much larger than that with NaCl solution and NaOH solution,[96] indicating that the ion adsorption model cannot fully explain CE between water and PTFE. At the same time, the signal of PTFE in contact with HCl solution showed a large peak value near

6.2 ppm, which was caused by the chemical shift relative to water, which was also related to the large amount of $H^+$ ions adsorbed on the surface. When the acid solution contacted PTFE, electron transfer and hydrogen ion adsorption occurred simultaneously, but the high concentration of hydrogen ions adsorbed on the SURFACE of PTFE inhibited the electron transfer between water molecules and PTFE. These NMR spectra agree well with the model presented in Fig. 5D.

Zhan et al. designed a sliding type TENG to study electron transfer at the polymer–liquid interface, as shown in Fig. 6A, which can further reveal the dynamic interaction between droplet and solid surface.[97] Here, PTFE films are also used for contact electrochemistry, where water droplets can easily slide off the slanted PTFE film surface. As shown in Fig. 6A, the droplets first spread into a cone and then slide across the surface until they separate from the ends. As shown in Fig. 6B, the induced charge generated by the interaction between DI droplet and fresh PTFE polymer is continuously recorded. According to TENG's working mechanism,[97] electrostatic shielding of charged surfaces by droplets neutralizes charges in overlapping regions, which also causes currents in external circuits (the detailed circuit can be seen in the reference paper). Thus, the amount of induced tribo-charge on the droplet can be determined by the difference between the two charge transfer processes (contact and separation). For the first droplet, a charge of 0.2 nC was observed when the droplet first came into contact with the polymer surface (Fig. 6B) due to the screening effect of the droplet. Then, an amount of charge (negative charge) of 2.6 nC was recorded as the droplet slid out of the surface, indicating that an amount of negative charge (difference between two signals) of 2.4 nC was induced on the PTFE surface due to the CE effect. On the other hand, as the number of droplets increases, the negative charge accumulated on the polymer surface reaches saturation. As shown in Fig. 6B, the induced charge on the droplet remains constant at the saturation stage, about 1 nC after about 80 droplets. It should also be pointed out that although the electrostatic charge generated on the droplet is quite small, the shielding effect of the droplet is quite strong in the saturated state and a significant current can be generated for energy collection as shown in Fig. 6B. Thus, the charge curve in Fig. 6B appears to be a square wave with a total charge of about 51 nC on the surface.

In order to clarify the contribution of the electron transfer effect, a series of "immersion-drop" experiments were carried out, in which PTFE films were immersed in different solutions to fully adsorb ions prior to the application of water droplets. In this case, the initial state of the PTFE surface may change due to the maximization of ion adsorption process. As can be seen from Fig. 6C, the saturation charge of the alkali treated PTFE (for 250 droplets) is about 70% of that of the original PTFE (untreated sample), meaning that CE still occurs between the water and the treated polymer film. If ion adsorption is the dominant effect of CE between liquid and solid, this immersion treatment should significantly reduce the amount of saturated charge on The PTFE surface. However, the results in Fig. 6C show that immersion treatment has limited influence on this experiment. Therefore, CE in this experiment may be related to the mixed effect of ion adsorption and electron transfer.

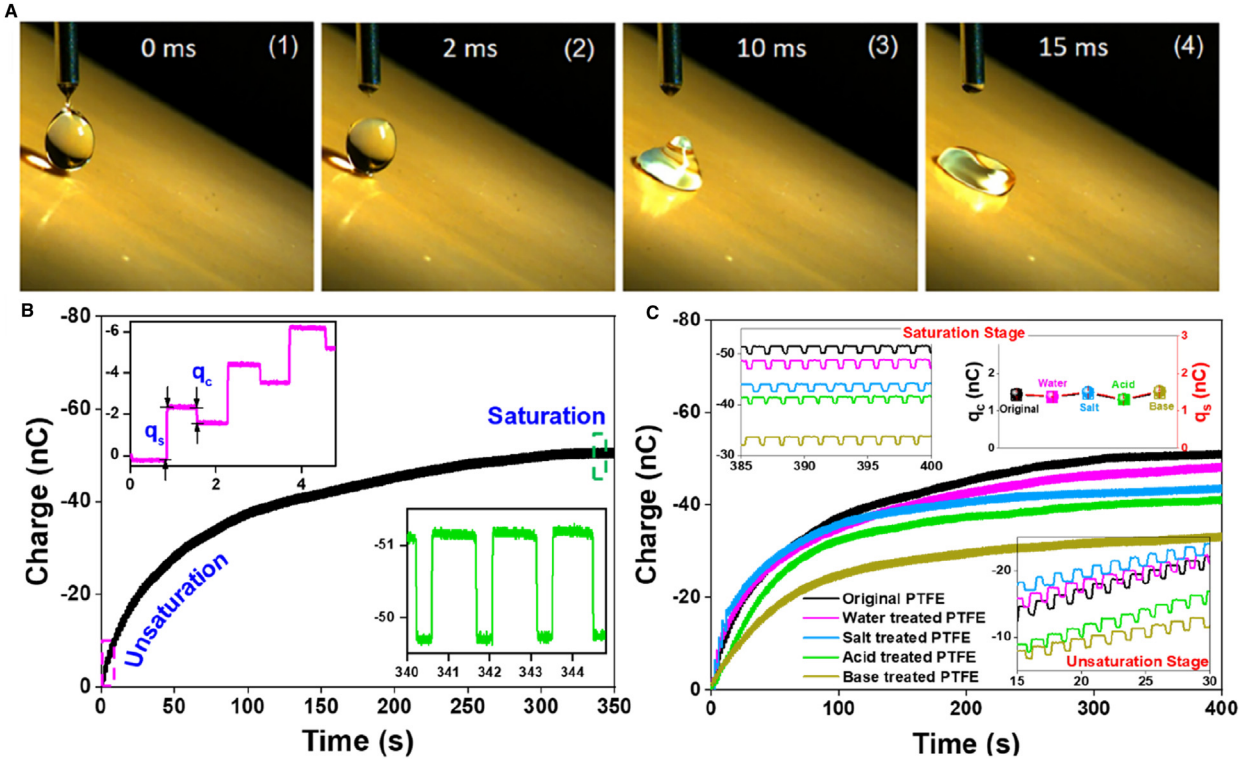


**Fig. 6** A sliding type TENG for studying the continuous electrification process between liquid and solid surface.[97] (A) the sliding motion of the droplet on the PTFE surface, (B) the charge saturation process on the PTFE surface and the insert is the detailed charge transfer process at the beginning state and saturated state, (C) the soaking experiments, where the PTFE surface is previously immersed in different liquids before the electrification test. Reproduced from Ref. 97. Copyright 2021 America Chemical Society.

Based on these experiments, it has been found that the working mechanism of TENG is very suitable for studying the physical processes at the liquid–solid interface. The TENG device can be used as a probe to detect charge generation and transfer (see Fig. 7). Tang et al. first reported a liquid metal-based TENG, which aims to achieve high power generation through complete contact between metal and dielectric.[123] In general, 100% contact cannot be achieved with TENG from solid materials, considering the roughness of the surface. Therefore, liquid metal applications can solve this problem. High output charge density of 430 $\mu Cm^{-2}$ and power density of 6.7 $Wm^{-2}$ can be achieved with this device. This idea was subsequently developed as a detection method for determining the electrochemical series of different dielectric materials. Zou et al.[124] introduced a standard method for quantifying the tribo-electric series of various polymer materials based on the contact electricity between the material being measured and the liquid metal. The proposed method uses TENG as a charge probe to uniformly quantify the surface charge density of general materials, which can reveal the intrinsic properties of polymers that gain or lose electrons. In addition to liquid metals, similar TENG systems can be used to study the electrochemical capabilities of different liquids, as we have described in the previous section.[97] Fig. 7 also shows a TENG array for detecting the dynamic output of a droplet during sliding on a solid surface. This design can show detailed interactions between the droplet and a large solid surface. This single-electrode type of TENG has a very high sensitivity for detecting induced charges at the liquid–solid interface,[125] calibrating charges up to pC level. In addition, combined with high-speed video, TENG's dynamic electrical output under different shock conditions allowed us to describe the electrical reaction quantitatively without any fitting parameters.[126] By matching the evolution of the hydrodynamic diffusion process with the time scale of the external electrical signal, it is possible to derive many liquid–solid electrochemical ratio laws. Similar applications of TENG as a charge probe can also use different modes of TENG, such as free-standing TENG[127] or even liquid film TENG,[24] which can be used as a sensor or electrostatic charge filter to accurately measure the surface charge of a target object. Therefore, TENG is a powerful technique for studying electrical interactions between liquids and other objects due to its high sensitivity and diverse structural design, and many new advances can be expected in the near future.

In addition to experimental studies, some theoretical calculations support that electron transfer can occur at the liquid-insulator interface. Willatzen et al. developed a quantum mechanical model for predicting electron transfer in CE for different material

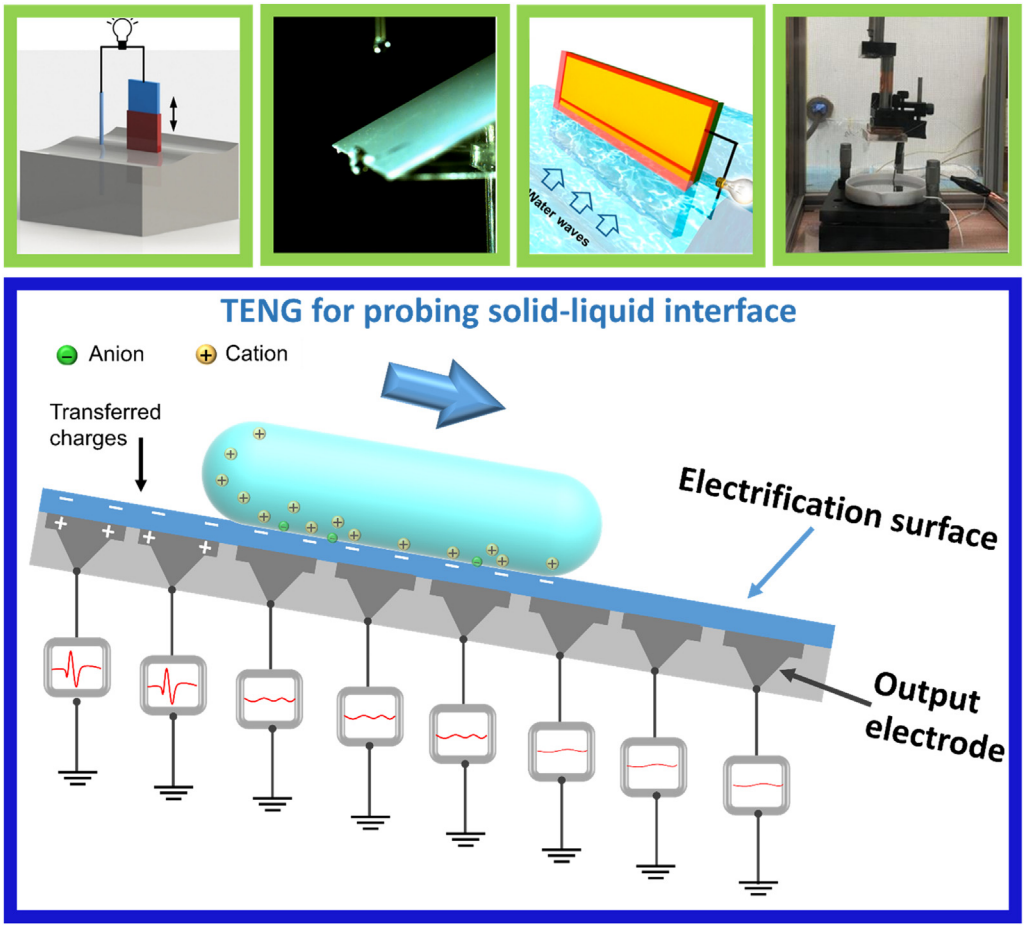


**Fig. 7** The research strategy for using TENG as a probe to study the charge generation on liquid–solid interface.[86,97,123,124] Reproduced from Ref. 86. Copyright 2014 America Chemical Society; Reproduced from Ref. 97. Copyright 2021 America Chemical Society; Reproduced with permission from Ref. 123. Copyright 2015 Wiley; Reproduced with permission from Ref. 124. Copyright 2019 Nature spring.

systems, including liquid–solid cases.[128] In quantum mechanical models, ion transfer is not considered, but electron transfer appears to be sufficient to support CE between liquid–solid CE. Li et al. studied CE between metal and amorphous polymer with a first-principle approach when water layer is present at the interface.[129] The results show that electrons transfer at the metal-water interface and polymer–water interface. More recently, Sun et al. quantified electron transfer in liquid–solid systems in different oxides based on density functional theory (DFT).[130] Different liquid–solid systems were established, in which the solid was diamond carbon, dielectric insulator ($SiO_2$), metal oxide ($TiO_2$ and $HfO_2$), and the liquid was water, as shown in Fig. 8A–D. The total state density (TDOS) at the liquid–solid interface was used to evaluate the charge transfer behavior. The influence of ionic solution concentration on liquid–solid CE was studied by introducing Na ions into liquid–solid interface. Two different calculation methods are used to reveal electron transfer in solid valence band (VB). One is the change in the number of electrons in the entire

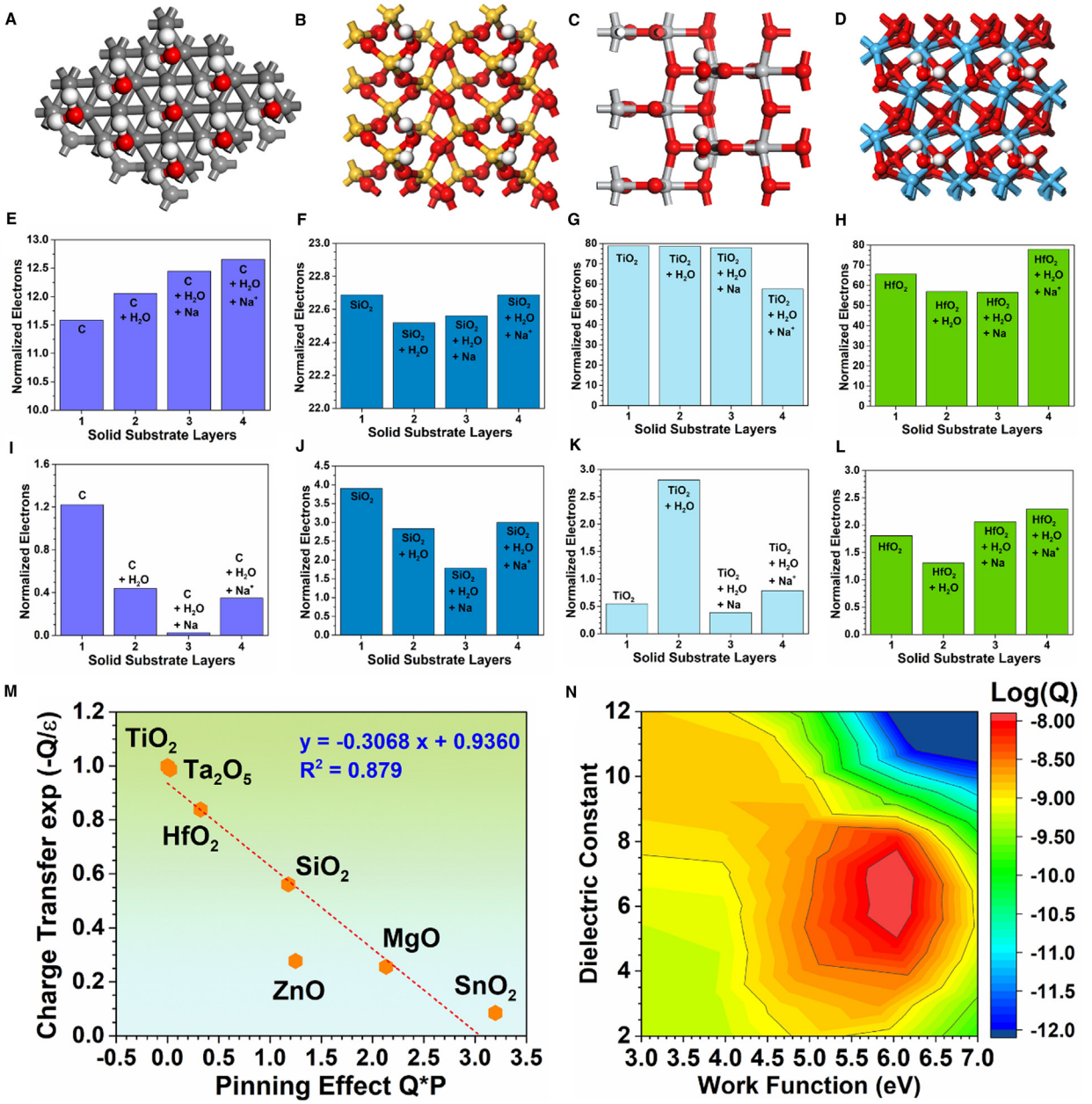


**Fig. 8** The DFT studies on the liquid–solid CE.[130] Different calculation models (A) diamond carbon-water, (B) $SiO_2$-water, (C) $TiO_2$-water and (D) $HfO_2$-water. The normalized electron numbers of the valence band for (E) diamond carbon, (F) $SiO_2$, (G) $TiO_2$ and (H) $HfO_2$ in contact with water and solution. The normalized electron numbers near the Fermi level for (I) diamond carbon, (J) $SiO_2$, (K) $TiO_2$ and (L) $HfO_2$ in contact with water and solution. (M) The linear correlation between charge transfer and dielectric function that is based on the introduction of the pinning factor. (N) The effects of dielectric constant and work function on the charge transfer at liquid–solid interfaces. Reproduced with permission from Ref. 130. Copyright 2021 Nature spring.

valence band of the solid, and the other is the change in the number of electrons in a small area near the Fermi level. Fig. 8E and 8L shows the change of the normalized electron number in the whole VB and the change of the electron number in a small range near the Fermi level when solid is in contact with water or ionic solution. The charge transfer between aqueous solution and different solids has been proved to be strongly related to the vacuum degree and Fermi level change of solid surface in contact with aqueous solution. It is proved that Na ion causes the band shift, which leads to the change of liquid–solid electron transfer. In addition, a linear relationship between liquid–solid electron transfer and dielectric function was found (Fig. 8M). The influence of dielectric constant and work function on charge transfer of solid surface is shown in Fig. 8N. DFT studies show that liquid–solid CE is a complex phenomenon, which can be affected by contact Angle, dielectric function, temperature and ion concentration. It should be mentioned that all these first principles calculations are based on electron transfer, which is consistent with the experimental work on electron transfer.

### Liquid-semiconductor contact electrification

Recently, the solid–solid CE involving semiconductors was found to generate directly current with a high current density.[131–133] Wang et al. pointed out that the generation of the direct current at the semiconductor interfaces is similar to that occur in the photovoltaic effect.[56] When a P-type semiconductor slides over a N-type semiconductor, the released energy "quantum" will be released at the interface due to the formation of new chemical bonds. The released energy can excite electron–hole pairs at the interface, which are further separated and moved from one side to the other side under the built-in electric field at the semiconductor interface, generating a direct current in external circuit. This phenomenon is analogous to photovoltaic effect and named as "tribovoltaic effect".

The photovoltaic effect cannot only occur at solid–solid interface, but also at aqueous solution and solid semiconductor interface, in which the aqueous solution is considered as a liquid semiconductor.[46–49,134] It implies that the tribovoltaic effect may also occur at the aqueous solution and solid semiconductor interface, since the tribovoltaic effect is similar to the photovoltaic effect. As shown in Fig. 9A, Lin et al. used a syringe conductive needle to drag a DI water droplet to slide over a silicon surface.[135] Fig. 9B shows the short-circuit current between the conductive needle and the P-type silicon wafer. The positive current was found to be generated when a DI water droplet slides over the P-type silicon surface, which implies that the electrons moved from P-type silicon side to the DI water side at the interface. When the DI water droplet slid on the N-type silicon surface, a negative tribo-current was generated and the electrons moved from N-type silicon side to the DI water side at the interface. The direction of the tribo-current was found to be consistent of the direction of the built-in electric field at the water and silicon interface. Further, Zheng et al. investigated the tribovoltaic effect at the liquid–solid interface under light irradiation.[136] It was revealed that the tribo-current between DI water and silicon wafer can be significantly enhanced by light irradiation, due to the increasing of the electro–hole pairs at the interface. These studies proved that the tribovoltaic effect can occur at the liquid–solid interface.

In the liquid-semiconductor tribovoltaic effect, the energy to excite the electron–hole pairs is also considered to come from the formation of the chemical bond at the interface. As shown in Fig. 9C, when a water droplet slides over a semiconductor surface, some water molecules will contact the fresh surface, forming chemical bonds and releasing energy, and the released energy "quantum" was named as "bindington". Fig. 9D give the whole process of the tribovoltaic effect at the liquid–solid interface. When a liquid and a solid semiconductor contact with each other, the built-in electric field will exist at the interface due to the difference in the Fermi levels. If the liquid starts to slide on the solid semiconductor surface, the bindington will be released and electron–hole pairs will be excited at the interface. Driven by the built-in electric field, the electron–hole pairs are separated and move from one side to the other side, generating a continuous direct current in external load.

Though the mechanism of the tribovoltaic effect at the liquid-semiconductor is different from that of the CE between liquid and insulator surface, the charge carries in the tribovoltaic effect are also electrons, which implies that the tribovoltaic effect at the liquid–solid interface also support the "two-step" model about the formation of the EDL, in which the electron transfer between liquid and solid is the first step.

### Liquid-metal contact electrification

In the tribovoltaic effect at the DI water and silicon interface, the DI water is considered as a semiconductor. It means that the junction between the DI water and silicon corresponds to a PN heterojunction. In solid–solid cases, the tribovoltaic effect was demonstrated to exist not only in PN junctions, but also in Schottky junctions, which are usually at the semiconductor–metal interfaces.[137] Therefore, the tribovoltaic effect should also exist at DI water and metal interfaces, which correspond to the Schottky junctions. As shown in Fig. 10A, the Fermi level of the metal is lower than that of the DI water. When they come into contact, a built-in electric field will be established to compensate for the difference in Fermi level (Fig. 10B). In the Schottky junctions, the depletion region is always at the semiconductor side in solid–solid case. It suggests that the depletion region should be in DI water side in the DI water-metal junction, which implies that the EDL at the metal and DI water interface can be considered as the depletion region in liquid-metal cases. Recent experimental works have proven that the tribovoltaic effect also exists at the metal and DI water interface.

In addition to the tribovoltaic effect, in which the transferred electrons are from the excited electron–hole pairs, charge transfer in the traditional sense can also occur between metals and liquids. As shown in Fig. 10C, the first-principle calculations shown that when the water contact a metal surface, such as Pt, the electron will directly transfer from one side to the other side at the interface.[138] The charge transfer at the water-metal interface is of significant interest not only in liquid–solid CE, but also in the studies

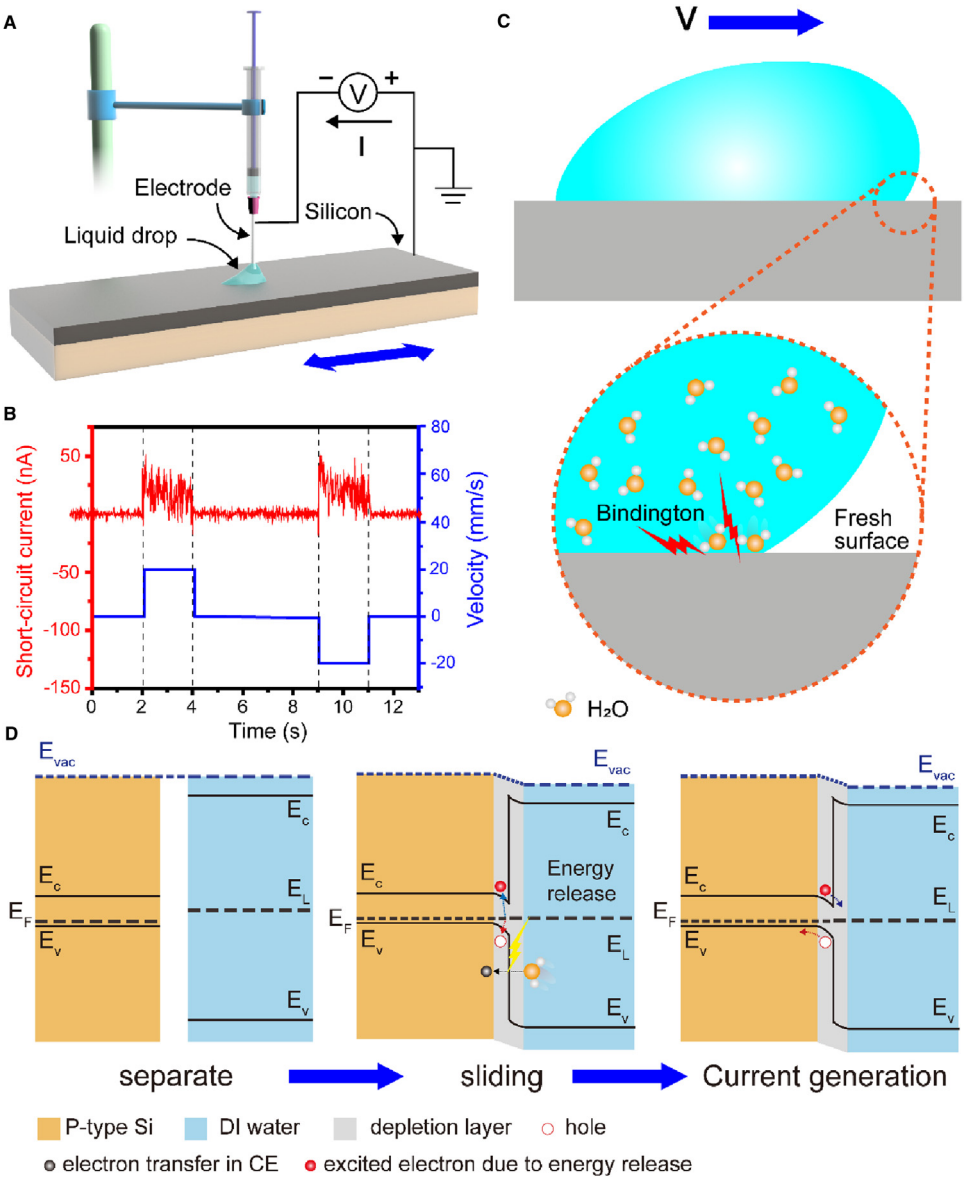


**Fig. 9** The tribovoltaic effect at the liquid-semiconductor interface.[135] (A) The setup of the tribovoltaic experiments and the external circuit. (B) The oscillogram of tribo-current when a DI water droplet slides on the P-type silicon wafer. (C) The generation of the "bindington" at the sliding water and semiconductor interface. (D) Energy band diagram of the tribovoltaic effect at a liquid–solid junction. Reproduced with permission from Ref. 135. Copyright 2021 Elsevier.

about corrosion and catalysis *etc.* in which the charge transfer is a fundamental issue. Anyway, in both the tribovoltaic effect and the direct charge transfer at the liquid-metal interface, the charge carriers are identified to be electrons when the metal is involved.

## "Wang transition" for CE

The above work suggests that electron transfer is dominant in liquid–solid CE, which raises a question. What are the conditions for electron transfer in CE? The "Wang transition" model of contact electrochemistry provides an answer to this question.[98] As shown in Fig. 11A, there is a distance a between atom A and atom B that keeps the two atoms in balance. When the distance between two atoms is greater than the equilibrium distance, they will attract each other (Fig. 11B). Conversely, if the distance between the two atoms is less than the equilibrium binding distance, the electron clouds of the two atoms will overlap and they will repel each other (Fig. 11C). Based on experimental data, Wang et al. pointed out that electron transfer in CE can only occur when the electron clouds of two atoms overlap.[98] As shown in Fig. 11D, the highest occupied energy level of the atom belonging to material A is higher than that of the atom belonging to material B. In this case, electrons don't go from atom A to atom B, because there's A high barrier

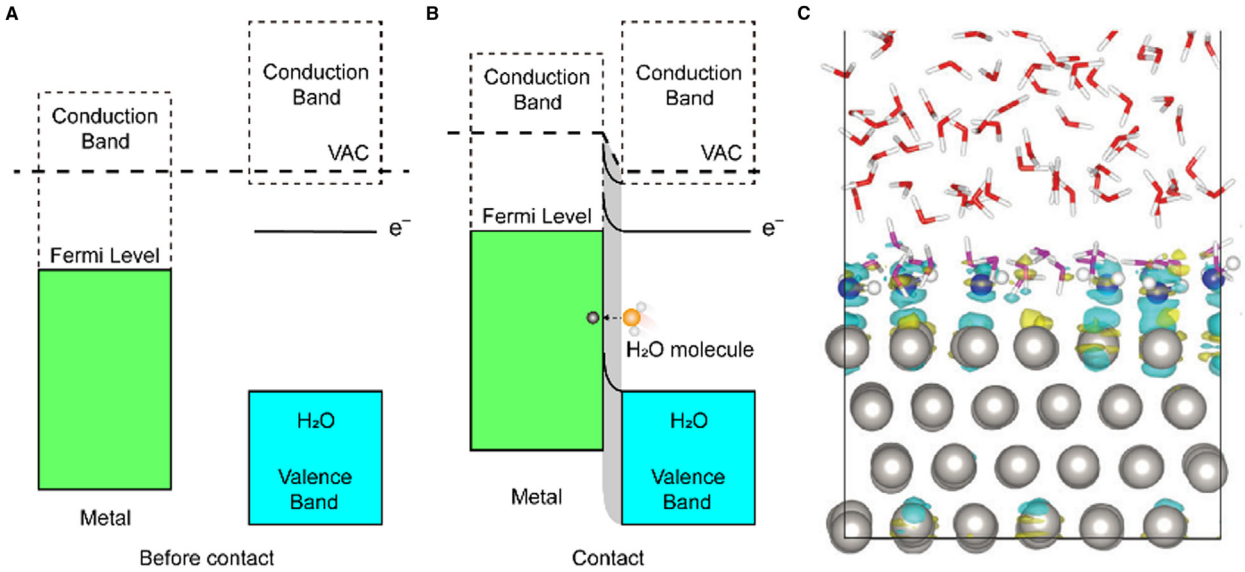


**Fig. 10** The tribovoltaic effect at the liquid-metal interface. (A) Energy band diagram at a liquid–solid junction before contact and (B) after contact. (C) The first-principle calculation about the electron transfer at water and Pt interface.[138] Reproduced with permission from Ref. 138. Copyright 2018 Royal Society of Chemistry.

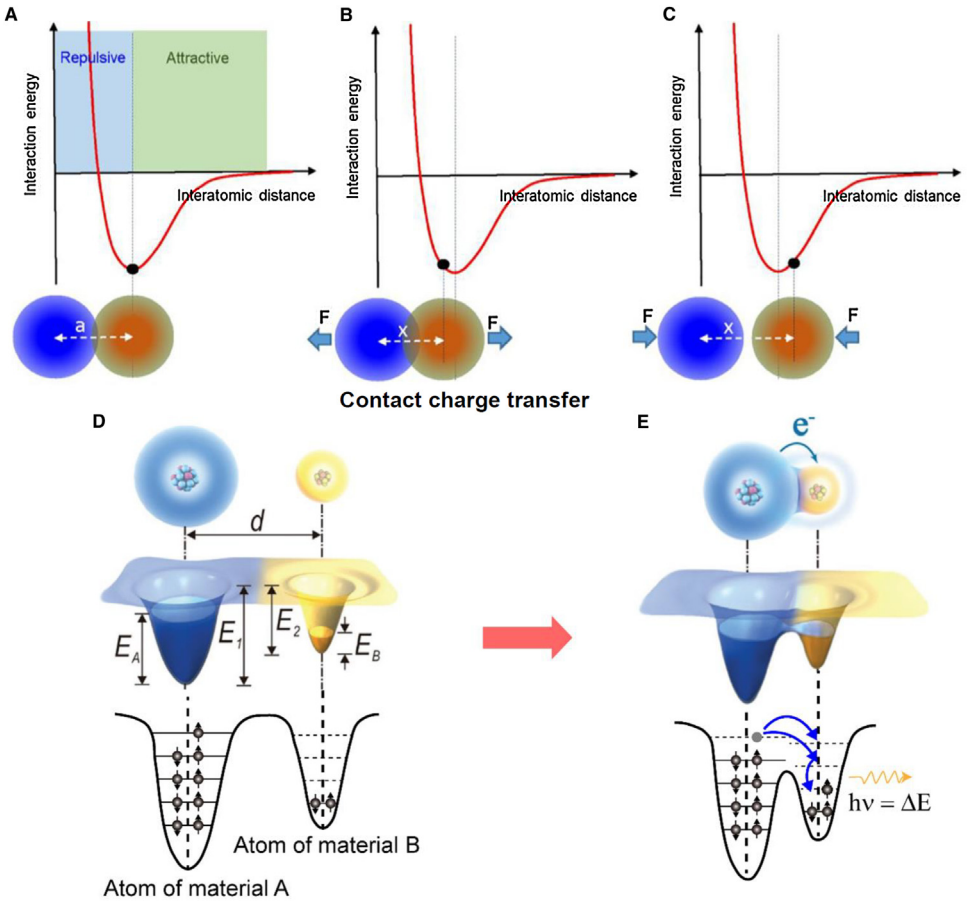


**Fig. 11** "Wang transition" model for contact electrification.[56,98] The interaction of two atoms at (A) equilibrium position, (B) attractive position, (C) repulsive position. The schematic of the energy diagram of two atoms (D) before contact, (E) in contact, and the photon emission is observed experimentally due to the hopping of electrons. Reproduced with permission from Ref. 56. Copyright 2019 Elsevier; Reproduced with permission from Ref. 98. Copyright 2019 Wiley.

between them. When the two surfaces are in close contact, the electron clouds of atom A and atom B overlap, reducing the barrier and transferring electrons from atom A to atom B, which can be simply called the "Wang transition" (Fig. 11E). Here, electrons can be transferred to any energy level of atom B below the highest placeholder energy level of atom A. The electrons will then move further to the lowest unoccupied energy level of atom B and release the photon, which has been observed experimentally. The overlap of the electron clouds, which provides a pathway for electron transfer in CE, can be thought of as forming a bond that is much longer than a conventional bond. When the two surfaces separate after contact, atom A, which has lost its electron, is dragged by other atoms on the surface of material A, the length of the bond between the two atoms (atom A and atom B) is lengthened and eventually broken, and atom A is separated from atom B, forming CE. But in some cases, the attraction between atom A and atom B is stronger than the attraction between atom A and the surface of material A, and the bond between the two atoms (atom A and atom B) becomes stronger, and atom A remains on the surface of material B, forming A new true bond and chemical reaction takes place. In these cases, CE cannot be detected because the entire neutral atom is transferred from surface A to surface B. The Wang transition model is verified by experiments and theoretical studies. Lin et al. investigated CE between Pt coating and $Si_3N_4$/AlN by using tapping mode AFM in different regions of needle–sample interaction (repulsion or attraction).[139] It is found that CE between tip and sample can only occur when tip and sample interact in the repulsive region, which is consistent with the Wang transition model. Willatzen et al. provided the first quantum mechanical calculation of electron transfer between two different atoms. The results also show that the overlap of the electron clouds belonging to two contacting atoms is a necessary condition for electron transfer.[140]

The Wang transition model can explain CE in any cases, including liquid–solid cases. Owing to liquid pressure, the liquid molecules will collide with atoms on the solid surface at a liquid–solid interface. The collision between liquid molecules and the atoms on the solid surface may lead to the overlap of electron clouds and result in electron transfer. In some cases, the atoms, which receive/lose electrons from/on the solid surface, are dragged away from the solid surface by other molecules in the liquid. The transferred electrons are left on the solid surface, resulting in traditional liquid–solid CE. But some time, the atoms belonging to the liquid molecules may form a new bond with the atoms belonging to the solid surface. In these cases, the bindington will be released, if the solid is metal or semiconductor, tribovoltaic current will be generated.

## Triboelectric nanogenerator based on liquid–solid contact electrification

Contact electrification at the liquid–solid interface is a persistent tough problem in the chemical-physical field, and lately, it has notably aroused the interest of researchers from a variety of fields. The rapid growth of L-S TENG is one of the main reasons for this situation. Enormous mechanical energy is contained in the ambient water movements, such as river flows, ocean waves, and even raindrops, and TENG capable of harvesting energy from these motions is a promising approach for on-site energy needs. Traditional energy harvesting techniques rely on electromagnetic generators[141,142] or piezoelectric generators, both of which have their limitations in harvesting energy from liquid–solid motion, such as size limitations, structural complexity, or low conversion efficiency. Therefore, TENG devices, with their benefits of compact size, simple system, low cost, and direct interaction with water bodies, might be a key strategy for resolving challenges in this field. The working mechanism of L-S TENG, which is based on a combination of electrification and electrostatic screening effect, has been comprehensively investigated by many earlier works.[83–94] Fig. 6B demonstrates the specific differences between these two effects. The essential ingredient is the electricity between a flowing liquid and a solid surface, thus the TENG structure can be single-electrode or free-standing mode. In 2013, Lin et al. reported the first L-S TENG based on a single electrode type structure.[83,92] Subsequently, many other researchers have also developed free-standing mode TENG for collecting energy, which relies mainly on the shielding effect of the liquid.[143,144] Last year, a novel transistor-inspired L-S TENG based on the bridging phenomenon between an electrification surface and an Al electrode was reported by Wang et al.[145] The diffusion of water droplets over the electrification surface in this device can convert the traditional interfacial effect into a bulk effect, resulting in remarkably high instantaneous power density. One hundred commercial LEDs can be powered by one drop (100.0 μL), which is the highest performance of L-S TENG to date. Therefore, a series of fresh breakthroughs are also expected soon as the basic research on S-L electrification progresses. Moreover, Wang et al. developed a unique slippery lubricant-impregnated porous surface-based TENG (SLIPS-TENG) to counteract the rapid degradation of interfacial materials' triboelectric properties in harsh conditions. The SLIPS-TENG is currently one of the growing fields of liquid–solid contact electrification, removing many of the inherent challenges encountered in the current TENG.

As illustrated in Fig. 12, the design of L-S TENG for energy harvesting may now be briefly classified into three categories. Firstly, the L-S TENG can be used to harvest energy on large surfaces (Fig. 12A), such as windows,[145,155] building walls,[155,156] *etc*. For instance, Liang et al. developed a multi-unit transparent TENG that can be directly used on a car window with an instantaneous power density of 12.66 mW $m^{-2}$.[145,155] Meanwhile, Choi et al.[155,156] studied an L-S TENG prepared surface nanostructures in reference to the natural surface of lotus leaves. This TENG can operate for 28 days without performance deterioration in the presence of a fluorinated electrification surface with high hydrophobicity.[155,156] Zhong et al. developed a multilayer L-S TENG with fine electrode arrays aimed for droplet or stream energy,[146,156] allowing the complete conversion of gravitational potential energy into electricity. Apart from raindrops, similar L-S TENGs can be utilized to harvest energy from ocean waves and currents as well. The design of L-S TENG for water wave energy uses a free-standing electrode array to create a continuous displacement current, which is basically identical to that for raindrops energy.

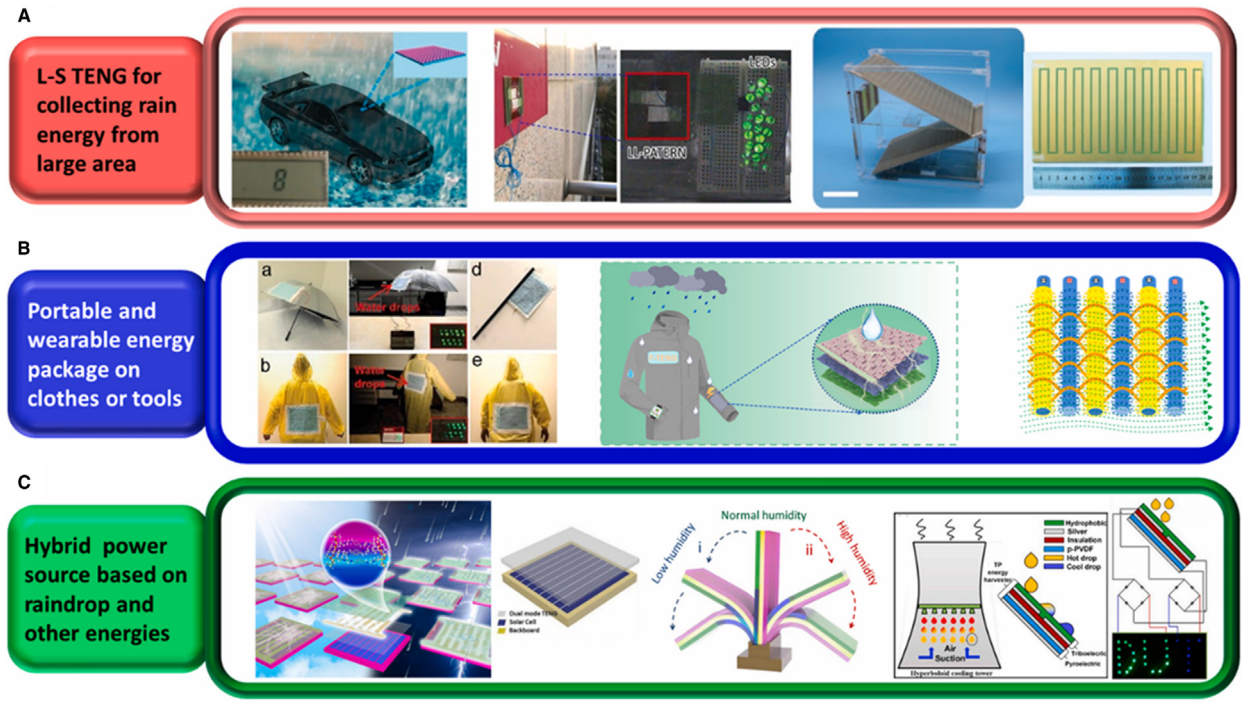


**Fig. 12** The application of L-S TENG for energy harvesting. (A) Energy collection on large surface.[146,147] (B) Portable and wearable energy package.[148–150] (C) Hybrid power source.[151–154] (A) Reproduced with permission from Ref. 146. Copyright 2016 Elsevier; Reproduced with permission from Ref. 147. Copyright 2017 Elsevier. (B) Reproduced with permission from Ref. 148. Copyright 2020 Royal Society of Chemistry. Reproduced with permission from Ref. 149. Copyright 2017 Wiley. Reproduced from Ref. 150. Copyright 2018 American Chemical Society. (C) Reproduced with permission from Ref. 151. Copyright 2021 Elsevier. Reproduced with permission from Ref. 152. Copyright 2015 Wiley.; Reproduced from Ref. 153. Copyright 2019 America Chemical Society; Reproduced with permission from Ref. 154. Copyright 2020 Elsevier.

The charge density and hydrophobicity are two main parameters that impact the performance of energy generation on the L-S TENG electrification surface. In fact, an increase in hydrophobicity does not always lead to a rise in charge density. Many studies have found that excessively increasing the roughness and contact angle suppresses transferred charges.[146,147,157] Increased surface roughness leads to increased hydrophobicity in hydrophobic materials, but it may also reduce the effective contact area between the droplet and the surface (the liquid cannot fully penetrate the inhomogeneous surface at the microscale). The high hydrophobicity, on the other hand, allows liquids to travel smoothly on a solid surface, whereas the current output of TENG is proportional to the motion velocity, implying that the high hydrophobicity is suitable for creating high current signals. Therefore, for L-S TENG, an appropriate hydrophobicity (neither extremely high nor extremely low) is critical, and this value must be custom-designed for various devices. Furthermore, modifying the electrification surface of L-S TENG by the charge injection treatment is another commonly utilized approach.[157,158] Ion cannons or corona polarization are used to inject excessive charges into the solid surface, while the energy generation depends on the electrostatic screening effect induced by moving droplets (the solid charged surface is always saturated).[158,159] The solid material for the charge injection treatment should be electret materials, otherwise, the surface charge density would be lost throughout the process. A variety of electret polymers have been used in the study so far, including PTFE, FEP, CYTOP, etc. The polarity of the polymer molecules (the dipole moment, the density of the polar molecule, and so on) determines the surface charge density and its persistence following injection treatment. According to previous studies, CYTOP films with high-temperature polarization are currently the best choice for such L-S TENG.[158,159]

Secondly, as shown in **Fig. 12**B, one of L-S TENG's primary directions is the portable and wearable energy package. Zhao et al. produced a freestanding with bi-electrode that can be mounted on the surface of an umbrella, representing a typical application of the L-S TENG used as a portable energy package. The device produces an output power density of up to 1.838 W $m^{-2}$ when mounted on an umbrella,[159,160] which is enough to light up to 30 commercial led lights. Aside from umbrellas, raincoats and shoes are also suitable to integrate with TENG. Xiong et al. reported a wearable all-fabric-based TENG that can collect energy from water flow and act as a smart cloth.[160,161] Furthermore, by coating hydrophobic nanoparticles onto various fabrics as electrification materials, this fiber-based L-S TENG can also realize the additional function of self-cleaning. This L-S TENG can provide an instantaneous output power density of 0.14 W $m^2$, and it can gather both electrostatic and mechanical energy from water. On the other hand, as compared to the solid–solid case, the electrification on the S-L interface is often insufficient, especially when the device is totally immersed in the liquid. Hence, it is important to further improve the solid–liquid interaction for wearable L-S TENG devices, which

can be achieved by inducing more turbulences via micro turbulators on the electrification surface[148,161] or by designing some tiny drainage channel on the electrification surface to increase contact-separation motions between solid and liquid.[148,149]

Thirdly, the hybrid energy generator is an intriguing and well-studied research direction of TENG that aims to harvest diverse types of energy from the ambient environment. The L-S TENG has an excellent performance in collecting energy from raindrops and is suitable for being integrated into hybrid energy systems (see **Fig. 12**C). The universal capability of L-S TENG allows it to work in tandem with a variety of different types of energy harvesters. For example, a hybrid energy system based on solar cells and L-S TENG that can derive energy from both the sun and raindrops was first reported by Zheng et al.[149,150] The transparent TENG adheres to the top surface of the solar cell, and falling raindrops contacting the TENG surface can induce energy output. Taking account of the low efficiency of solar cells on rainy days, this hybrid system can effectively compensate for the energy loss of solar cells. Many advancements have been achieved since then for this solar-raindrop energy system. For example, different nano-patterns have been added to the TENG surface to improve the light absorption of solar cells.[151,152] For the fabrication of L-S TENG, self-healing and self-cleaning materials have been used, allowing the light transparency and long-term operation of solar cells to be further protected.[149,150] The L-S TENG can also operate with wind energy harvesters in addition to solar energy. Ren et al. reported an adaptive TENG that can exhibit spontaneous deformation at different humidity[152,162] (see **Fig. 16**C). The humidity-sensitive material is embedded into the junction site of TENG, while the humidity change leads to the banding of TENG to different positions. The TENG arrays are all erected on windy days with normal humidity, and their vibrations in the wind can generate electrical energy. Then, the TENG arrays are driven to lay down by the high humidity in the air during rainy days, which allows the electrification surface to capture raindrop energy based on the CE effect. Moreover, Jiang et al. presented a hybrid generator made up of a free-standing mode L-S TENG and a pyroelectric generator (PENG) for harvesting both thermal and kinetic energy from a thermal fluid.[162,165] Due to the CE effect related to ambient temperature, the output power of TENG decreases as droplet temperature rises. The hybrid energy harvester has a peak power density of 2.6 $\mu W\,cm^{-2}$ with a maximum energy increment of 238% over the pure PENG device, enabling the lighting of 28 commercial LEDs. With the help of a rectifier circuit or storage units, different energy generators can be combined to create hybrid energy systems with a higher unified energy density than a single unit. Despite the variety of different physical effects and mechanisms, the cooperation method between multiple generating units still needs to be further explored to harvest different environmental energy sources simultaneously and compensate for shortcomings of each unit.

Apart from energy harvesting, electrification on the L-S interface can also serve as a force-electricity conversion effect, which inspires a variety of different applications, as partially summarized in **Fig. 13**. One of the key research directions focusing on L-S electrification is fluidic sensors for sensing movements and deformations. For example, Shi et al. suggested a flexible pressure sensor in a microfluidic channel based on L-S electrification,[153,165] which can conformably work on human skin by combining the operating principles of electrification and capacitive variations. Dynamic pressure can be immediately revealed by the electrification between microfluidics and channel surface without external power supply, whereas capacitive change offers a complementing sensing method for distinguishing between dynamic and static pressure. This microfluidic sensor possesses the ability to simultaneously monitor the magnitude and frequency of pressure, making it ideal for tracking complicated human movements. The similar working principle can be adopted for underwater wearable electronics. Zou et al. developed a bionic L-S TENG that can collect energy from underwater

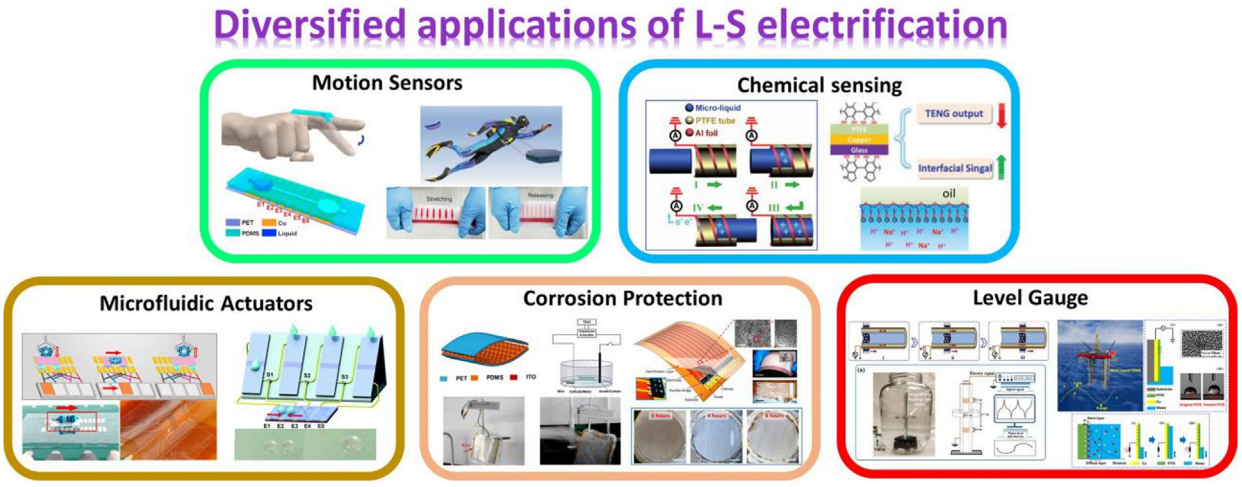


**Fig. 13** Diversified applications of liquid–solid contact electrification in addition to energy harvesting.[25,26,90,166–172] Reproduced with permission from Ref. 25. Copyright 2020 Elsevier; Reproduced with permission from Ref. 26. Copyright 2019 Wiley; Reproduced with permission from Ref. 90. Copyright 2019 Elsevier; Reproduced with permission from Ref. 166. Copyright 2016 Elsevier; Reproduced with permission from Ref. 167. Copyright 2019 Nature spring; Reproduced with permission from Ref. 168. Copyright 2017 Wiley; Reproduced from Ref. 169. Copyright 2018 America Chemical Society; Reproduced with permission from Ref. 170. Copyright 2018 Royal Society of Chemistry; Reproduced with permission from Ref. 171. Copyright 2015 Elsevier; Reproduced from Ref. 172. Copyright 2015 America Chemical Society.

movements by mimicking the ion channels of an electric eel.[153,154] The flowing liquid in the electrification channel produces an output voltage of over 10 V, which can be used to support body multi-position motion monitoring and an underwater rescue system. The electrification on the S-L interface can serve as a surface chemical sensor in addition to a fluidic motion sensor. Chen et al. designed a self-powered volume sensor capable of detecting both volume and conductivity based on L-S CE.[154,166] Furthermore, the ultrafine/highly flexible structure of the device allows it to be applied for microfluidic biological and chemical detection. Jiang et al. also reported the application of L-S TENG in identifying dopamine concentrations at liquid–liquid interfaces.[26] Moreover, given the precise control of the position and velocity of liquids in microchannels that can be achieved by electrowetting technique, various self-powered microfluidic systems can be realized by combining electrowetting technique and L-S electrification. For example, Nie et al. reported a mini delivery vehicle that uses four droplets to transport tiny objects at a maximum regulated speed of 1 m/s.[166,167] Chen et al. further proved that the induced electrical output from the electrification between a droplet and the TENG surface is sufficient to operate an electrowetting actuation matrix.[167,168] Corrosion prevention for ships or ocean machinery is another prospective application area for L-S CE. The L-S TENG can support a long-term corrosion prevention procedure without external power supplies,[169,170] and the mechanical energy can be easily obtained from ocean waves, suggesting that self-powered sensors based on L-S TENG may have enormous applications in ocean-related domains. For example, the level gauge based on L-S electrification can be used in various scenarios, such as cargo ships[25] or drilling rigs.[90]

## Revisiting the model of electric double-layer

### Hybrid EDL model and the "two-step" formation process

As presented in the preceding sections, the electron transfer process is a strong effect that deserves emphasis in the CE process between liquids and solids, and thus it should also be taken into account in the formation of the EDL. As shown in Fig. 14, the hybrid EDL model (simply called Wang's hybrid layer) and the "two-step" formation process are elaborated by Wang et al.[56] in 2018, which considers both electron transfer and ion adsorption (chemical interaction). For example, solid materials with strong electron capture abilities (e.g., polymers with a significant number of fluorine groups) can collect electrons directly from water molecules or even ions in the liquid. The liquid molecules near the solid surface can then be pushed away from the interface owing to liquid flow or turbulence. The electron transfer process is related to the hopping of electrons from higher to lower energy states. Thus, if the energy fluctuations of electrons (kT, where k is Boltzmann's constant and T is the temperature) are below the energy barrier (Ep), most of the electrons transported to the surface can be maintained. In the second step, due to the electrostatic interactions, free ions in the liquid can be drawn to the electrified surface to form an EDL, which is similar to the conventional EDL model (Fig. 14B). At the same time, ionization processes take place simultaneously on the solid surface, resulting in the generation

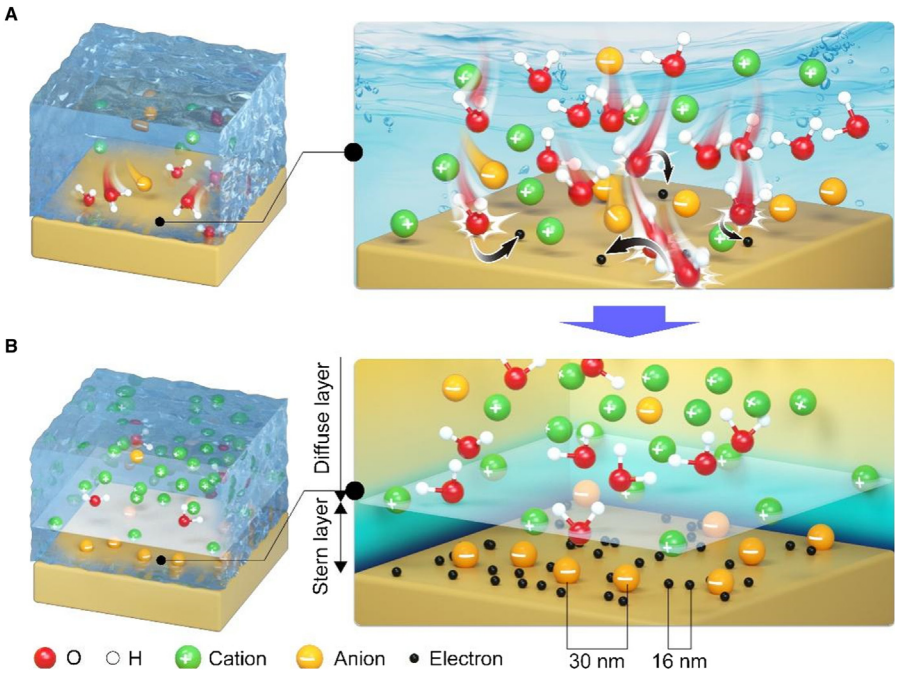


**Fig. 14** The Wang's hybrid EDL model and the "two-step" processes about its formation. (A) In the first-step, the molecules and ions in the liquid impact the solid surface due to the thermal motion and the pressure from the liquid, leads to the electron transfer between them, meanwhile, the ions may also attach to the solid surface. (B) In the second step, free ions in the liquid would be attracted to the electrified surface due to electrostatic interactions, forming an EDL.

of both electrons and ions. Furthermore, when a water molecule loses an electron, it transforms into a cationic of $H_2O^+$. The lifespan of $H_2O^+$ is proved to be shorter than 50 fs,[170,171] based on the chemical reaction[171,172]: $H_2O^+ + H_2O \rightarrow OH + H_3O^+$, $H_2O^+$ combines with an adjacent water molecule to produce an OH radical and $H_3O^+$. Therefore, the severed molecules that are pushed away from the solid surface become freely migrating ions in the liquid, which can also contribute to the formation of EDL.

For this hybrid EDL model, there are a few crucial aspects to emphasize. To begin with, both the ions created by the ionization process and the transferred electrons can alter the potential distribution near the surface, whereas the formation of the Stern layer and the diffusion layer in this hybrid EDL model shall have no substantial difference. The ionization at the liquid–solid interface induces more charges on the surface in the conventional EDL model, leading to the charge dispersion and compensation in the diffusion layer. In the hybrid layer, the charge transfer between solid and liquid molecules results in more charge accumulation on the surface. This electron transfer process is parallel to the ion adsorption, and in some cases, such as the CE between $SiO_2$-water and PTFE-water,[95,96] electron transfer plays a leading role in the generation of surface charges. The adsorption of ions can be divided into chemisorption and physisorption. Meanwhile, the different parts of the hybrid EDL model are related to the solid surface states. Transferred electrons are usually trapped in the surface state, whereas the extra charges generated in the ionization reaction are stuck in the atomic orbitals of the atoms. Thus, the potential barrier of the surface state should be lower than that of atomic orbitals, and the transferred electrons in the surface states should be mobile and relatively unstable, as demonstrated by the heating treatment experiment.[95] In addition, the capacity of solid materials to donate/withdraw electrons can determine the CE between solids, and this principle can also be extended to the CE between L-S.[22,173] For example, polymers with high EW properties (such as PTFE and FEP) can produce considerable electron transfer effects during CE with liquids, and the electrification performance can be further improved by intentionally adding certain unsaturated groups on the surface. Accordingly, the electron-donating/withdrawing capabilities of solid materials may affect the formation of the EDL, including the charge density and near-surface potential distribution. Besides, in liquid–solid CE, the electron transfer probability is usually less than one out of ~2500 surface atoms.[95] In the case of CE between $SiO_2$ and DI water, as can be estimated from the charge density, the distance between two neighboring electrons on the $SiO_2$ surface is 16 nm while is ~30 nm between two adjacent O- ions. The distances are substantially more than the thickness of the Stern layer,[173,174] therefore the EDL description should also take account of the distance between two adjacent charges, as illustrated in **Fig. 14**.

## Revisiting the EDL model and its related fields

The EDL model has been widely used in many fields, covering energy storage, electrochemical reactions, capacitive deionization, hydrogel ionization, electrophoresis, colloidal adhesion, and many other disciplines. However, as proposed in **Fig. 14**, the origin of EDL formation at the liquid–solid interface may have another possible explanation based on the electron transfer effect during liquid–solid contact. It is suggested to revisit the studies and applications related to EDL based on this hybrid electrification process (electron transfer and ion adsorption) on the S-L interface, as shown in **Fig. 15**. EDL capacitors[103] rely on charge accumulation in the EDL to store energy (**Fig. 15**A), while the EDL behavior on the electrode surface is usually determined by the external electric field, the kinds of electrolyte ions and the ion adsorption process. Then the interactions between the adsorbed ions and the electrode surface can be explained by chemical affinity. When considering electron transport between the electrode surface and the liquid molecule, we must further consider charge accumulation and dispersion near the surface. Although the electron transfer effect is pronounced at the polymer–liquid interface[22] and generally quite weak at the electrode-liquid interface, it remains necessary to consider it to complete the physical picture near the electrode surface. Previous research has shown that inserting electrorheological liquid crystal molecules into the electrolyte can reduce the self-discharge of EDL capacitors, where the surface potential can induce fluid viscosity to slow down the diffusion of ions.[175] It also indicates that in some circumstances, the electron transfer effect might provide a distinctive contribution. Similarly, both capacitive and pseudocapacitive processes of EDL have been shown to have a remarkable effect on electrocatalytic reactions (**Fig. 15**B),[182,183] where continuous EDL reconstruction can be seen by chemical phase modification. The existence of EDL and electrified interfaces can be used to explain the impact of cations on various experimental results,[183,184] where the local environment of catalysis also needs to be defined to include electrostatic interactions of ionic species with charged metal surfaces. In this context, the hybrid EDL model that includes the electron transfer mechanism can also contribute to the clarification of certain physical hypotheses related to experimental observations.

On the other side, mechanochemistry studies the effect of mechanical forces on the chemical bonding of force-reactive materials, which can potentially generate novel materials that cannot be obtained by other means. For example, Boswell et al.[185] used ultrasonication to generate force activation to synthesize a gold-colored, semiconducting fluoropolymer (fluorinated polyacetylene) (**Fig. 15**C), suggesting that polymer mechanochemistry is a viable synthetic tool for obtaining novel materials. The CE effect between L-S may also contribute to this process on this basis if we choose the appropriate materials to induce the electrons transfer on the interface. Furthermore, according to the DLVO (Derjaguin, Landau, Verwey, Overbeek) theory, the interaction of EDL has a significant impact on colloid particle adherence,[186] and this adhesion effect may also be used to manipulate bacterial cells.[176] The charge densities at bacterial cell surfaces are influenced by the local electric potential (**Fig. 15**D), which changes under the EDL interaction with another surface, leading to different adhesion behaviors of the bacterial cells. As demonstrated in prior studies,[180] the adsorption flux can be enhanced with dilute electrolytes owing to EDL interactions among particles. Besides, in previous studies, the EDL on the particle–liquid interface was calculated under the assumption that the particle surface has a constant charge density in the initial state, but no in-depth discussion on the origin of these initial charges. Thus, if referring to the hybrid EDL model in **Fig. 14**, it is likely that these initial charges are derived from the electron transfer process during contact,

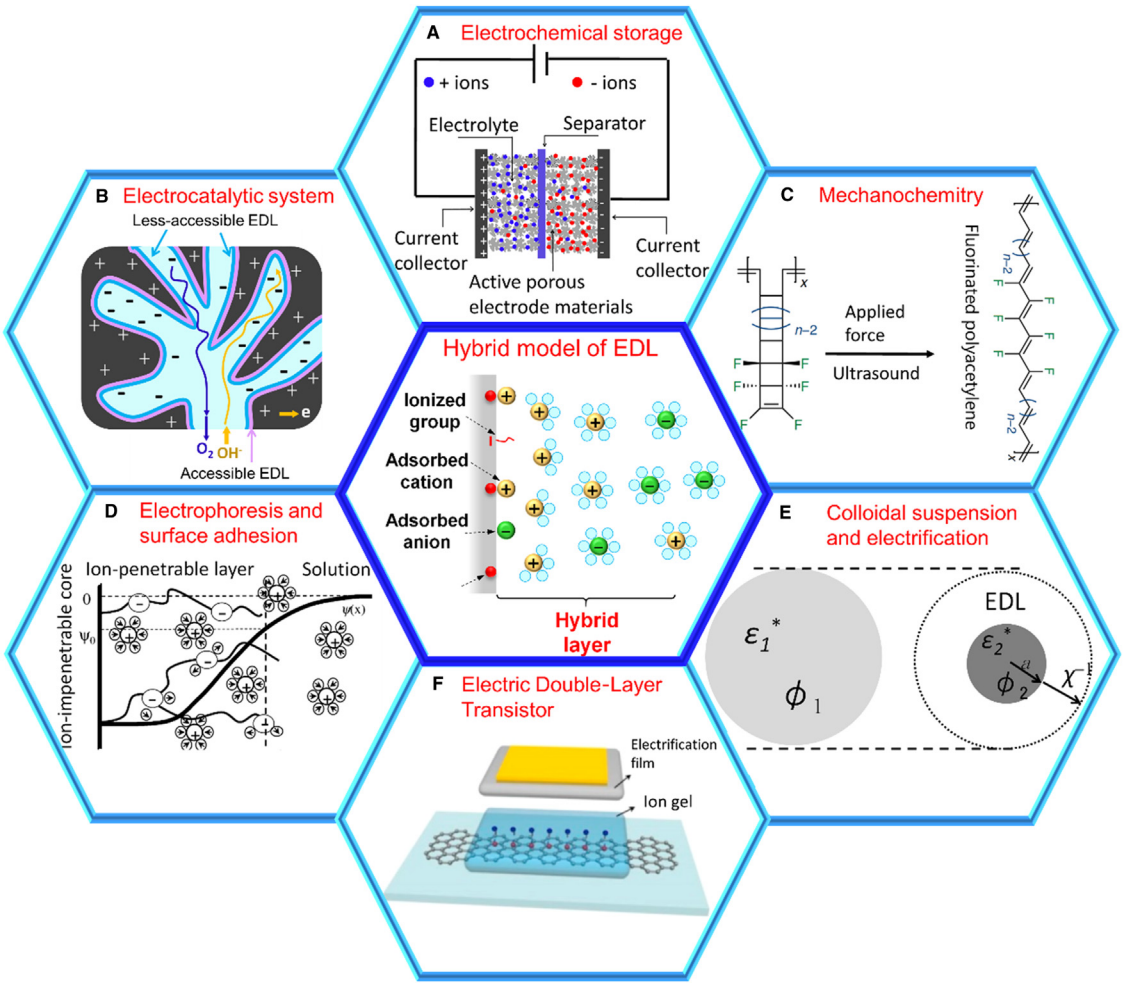


**Fig. 15** A revisit of EDL and its related fields. (A) electrochemical storage[103] (B) electrocatalytic system[175] (C) Mechanochemistry[176] (D) Electrophoresis and surface adhesion[177] (E) Colloidal suspension[178] (F) EDL transistor.[179] Reproduced with permission from Ref. 180. Copyright 2002 Elsevier; Reproduced from Ref. 181. Copyright 2018 America Chemical Society.

so that the calculation of the surface potential may also need to consider the CE effect between the particles and the liquid. As demonstrated in **Fig. 15**E a comparable case may be seen in the phenomena of colloidal suspension.[187] In addition, the EDL can act as a large-capacitance nanogap capacitor, allowing charge accumulation at L-S interfaces up to extremely high levels. Therefore, EDL transistors with ionic liquids or electrolytes as gate dielectrics[30] have been of great interest for their wide electrochemical windows, low vapor pressures, and good chemical and physical stability.[177] EDL transistors can be efficiently governed by triboelectric potential rather than applying gate voltages (see **Fig. 15**F), which can serve as mechanically sensitive electronics.[178] Ion gels are commonly used as the gate dielectric and electrification layer for human–electronics interaction, and the transistors can be controlled by voltage signals triggered by the contact electrification on the surface of the ionic gel.[188] In this case, the physical process occurring on the surface of the ionic gel should be further clarified based on the hybrid EDL model.

## Potential impacts of the hybrid EDL model to other energy generators

Apart from the mentioned study fields, there are many other energy harvesters that are also related to EDL. As is well-known, when a pressure-driven flow occurs in an aqueous solution in a channel with surface charges on its walls, a flowing current will be generated.[179,181,189] The reason can be explained that when the aqueous solution contacts the charged wall an EDL is formed, and the ions in the EDL will orientally move under the external pressure, generating a direct current. Various electric generators were constructed for collecting energy from the ambient environment based on the streaming current, as illustrated in **Fig. 16**A.[181] The streaming current may also be produced by dragging a liquid droplet over the graphene surface (**Fig. 16**B)[144,163] and even at the liquid–liquid interface.[190] The influence of different factors to improve the efficiency of energy harvesters has been discussed, including the thickness of the EDL, flow velocity, concentration, and so on.[179] In particular, as one of the key issues in the theory of hybrid EDL, the identification of the charges has drawn little attention on the surface of the wall until now. Various principles of

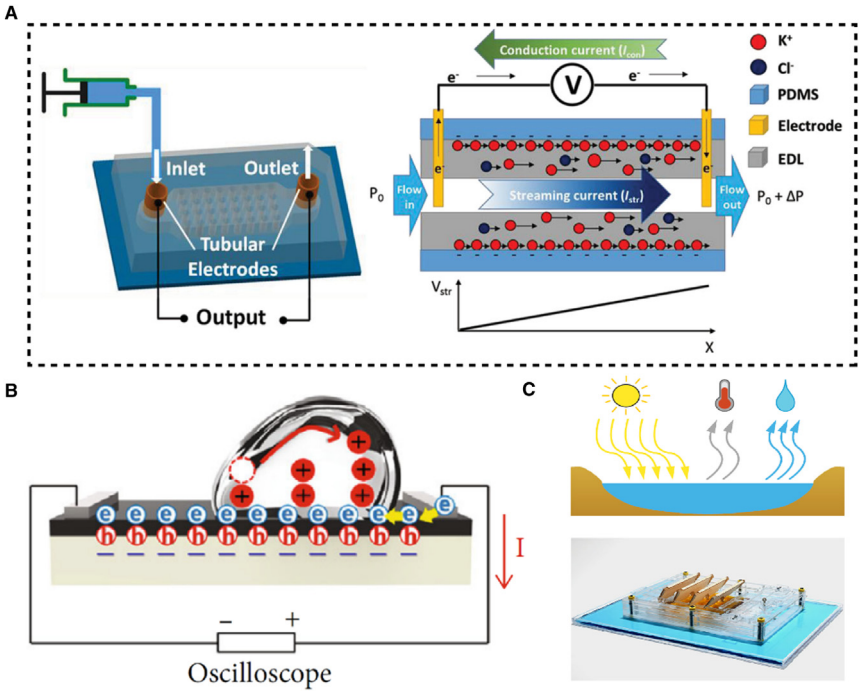


**Fig. 16** Impacts of hybrid EDL model on other energy generators. (A) and (B) Energy harvesting from streaming current.[144,163] (C) Energy harvesting from surface vapor evaporation.[164] Reproduced with permission from Ref. 163. Copyright 2015 Wiley; Reproduced from Ref. 144. Copyright 2016 America Chemical Society; Reproduced with permission from Ref. 164. Copyright 2017 Nature spring.

material selection for streaming current generators will be available based on different charge transfer theories (electron transfer or ion transfer). Besides, since it is easier to excite electrons compared to ions, it may be possible to improve the temperature stability of the generators by adjusting the ratio of ions to electrons. However, these issues have not to be addressed in the research of streaming current generators. Except for streaming current generators, various techniques based on charge transfer at the liquid–solid interface have been developed, including the electrokinetic energy device,[191] the fiber-shaped fluidic nanogenerator (FFNG),[192] the carbon-water device,[193] and so on. Recently, harvesting energy from evaporation has also attracted considerable attention (**Fig. 16**C).[194–196] Unlike in the liquid–solid CE, the liquid in these techniques remains in touch with the solid surface. But it is also essential to have electron transfer at the liquid–solid interface since the mechanism of these techniques is relevant to EDL as well. Therefore, it is possible that the "Wang's transition" model and Wang's hybrid EDL theory have implications for this technique.

## Conclusion and perspectives

In this review, we summarize recent work on mechanisms and applications of liquid–solid CE. Although charge transfer at liquid–solid interface is one of the key issues in many fields and CE has been studied for a long time, historically, liquid–solid CE has not received the attention it deserves. Due to the invention of liquid–solid TENG, liquid–solid CE was pushed to center stage. Two key problems of liquid–solid CE, namely, the properties of charge carriers and the formation of EDL, have been systematically investigated recently.

In the liquid–solid CE, the solids could be insulators, semiconductors or metals. For the liquid-insulator CE, we summarized several latest works that demonstrated the existence of electron transfer at L-S interface by using diversified methods in both micro-scale and large scale. In some cases, the electron transfer even plays a dominant role. The mechanism of the liquid-semiconductor CE is very different from that of the liquid-insulator CE. In the liquid-semiconductor CE, the electron–hole pairs are first excited by the energy released due to the forming of bonds at the interface, which can be called as "bindington". Then the electron–hole pairs are separated and directionally move from one surface to the other surface under the driving of the built-in electric filed at the interface, generating a direct tribo-current. This process is similar to the photovoltaic effect, so that it was named as the tribovoltaic effect. It is verified that the tribovoltaic effect also exist at the liquid-metal interface, in which the liquid, usually aqueous solution, is considered as the semiconductor. No matter the solid side is insulator, semiconductor or metal, the electron transfer plays an important role.

A newly proposed Wang transition model is also introduced in this review. In Wang transition model, the two atoms are close to each other, and the electron clouds belonging to the two atoms overlap with each other, reducing the potential barriers and resulting electron transfer. When they separate, the electrons belonging to one atom are left on the other atom, and the CE occurs.

In addition to the mechanism of the liquid–solid CE, recent progresses in the liquid–solid TENG and other applications related to this CE effect are also reviewed. Recent years, different liquid–solid TENGs were designed to harvest the energy from on large surface, or designed as portable and wearable energy package for electronics applications or even combined with other energy technique to establish a hybrid energy generator. We have summarized several key points for designing L-S TENG, including its operation mechanism and the methods of surface treatment. In addition to energy harvesting, CE on L-S interface can also be applied for sensors, reactors, manipulators and many ocean related devices. Furthermore, the L-S TENG can be a probe for probing the electrification at liquid–solid interface. With the further exploration of the fundamental physics of L-S electrification, a series of impacts in the related fields are expected in the future.

Based on the electron transfer, Wang et al. proposed a hybrid EDL model and a "Two-step" formation process, while we provide an in-depth explanation of this concept in this review. In the Wang's hybrid EDL model, the electron transfer due to the overlap of the electron clouds occurs in the first step. Further, the liquid molecules are pushed away from the solid surface, while the electrons remain. In the second step, free counter ions in the liquid are attracted, forming an EDL. A key difference between the hybrid EDL theory and traditional EDL theory is the identity of the charge carriers in the charged solid surface. The hybrid EDL model considers the electron transfer, while the traditional EDL model does not. The electron and ion are very different, for example, they are different in size, mass, mobility and diffusion range, and they need different energy to leave the surface. More importantly, the dynamics related to electrons and ions are very different, because electrons can be easily excited by raising temperature and/or photon excitation, so that they are easily leaked out from surfaces/interfaces, which may affect the charge storage capability. So far, the EDL related fields, such as electrochemical storage, mechanochemistry, electrocatalysis, electrophoresis etc., were based on the traditional EDL model, which may lead to unexplained phenomena. It means that the hybrid EDL model may have significant implications on the EDL related fields, which still remains to be further developed experimentally.

This review focus on introducing the works on liquid–solid CE. In fact, the liquid molecules will collide with each other at the liquid–liquid interface, and results in electron transfer as well. Therefore, the concepts and models introduced here for liquid–solid CE, such as the Wang transition model and Wang's hybrid EDL model, may also be suitable for liquid–liquid CE, which has attracted increasing attention. Experimental verification of the correctness of these models in liquid–liquid CE will be one of the key points in the future studies on the CE.

## References


1. Terris, B. D.; Stern, J. E.; Rugar, D.; Mamin, H. J. Contact Electrification Using Force Microscopy. *Phys. Rev. Lett.* **1989,** *63,* 2669–2672.
2. Gibson, H. Linear Free Energy Relations. V. Triboelectric Charging of Organic Solids. *J. Am. Chem. Soc.* **1975,** *97,* 3832–3833.
3. Sakaguchi, M.; Makino, M.; Ohura, T.; Iwata, T. Contact Electrification of Polymers Due to Electron Transfer Among Mechano Anions, Mechano Cations and Mechano Radicals. *J. Electrostat.* **2012,** *72,* 412–416.
4. Liu, C.; Bard, A. Electrostatic Electrochemistry at Insulators. *Nat. Mater.* **2008,** *7,* 505–509.
5. Diaz, A. F.; Wollmann, D.; Dreblow, D. Contact Electrification: Ion Transfer to Metals and Polymers. *Chem. Mater.* **1991,** *3,* 997–999.
6. McCarty, G. M.; Whitesides, G. M. Electrostatic Charging Due to Separation of Ions at Interfaces: Contact Electrification of Ions Electrets. *Angew. Chem. Int. Ed.* **2008,** *47,* 2188–2207.
7. Davies, D. K. Charge Generation on Dielectric Surfaces. *J. Phys. D. Appl. Phys.* **1969,** *2,* 1533–1537.
8. Duck, C. B.; Fabish, T. J. Contact Electrification of Polymers: A Quantitative Model. *J. Appl. Phys.* **1978,** *49,* 315–321.
9. Sutka, A.; Malnieks, K.; Lapcinskis, L.; Kaufelde, P.; Linarts, A.; Berzina, A.; Zabels, R.; Jurkans, V.; Gornevs, I.; Blume, J.; c Knite, M. The Role of Intermolecular Forces in Contact Electrification on Polymer Surfaces and Triboelectric Nanogenerators. *Energ. Environ. Sci.* **2019,** *12,* 2417–2421.
10. Pandey, R.; Kakehashi, H.; Nakanishi, H.; Soh, S. Correlating Material Transfer and Charge Transfer in Contact Electrification. *J. Phys. Chem. C* **2018,** *122,* 16154–16160.
11. Baytekin, H.; Patashinski, A.; Beanicki, M.; Baytekin, B.; Soh, S.; Grzybowski, B. The Mosaic of Surface Charge in Contact Electrification. *Science* **2011,** *333,* 308–312.
12. Lin, S.; Shao, T. Bipolar Charge Transfer Induced by Water: Experimental and First-Principles Studies. *Phys. Chem. Chem. Phys.* **2017,** *19,* 29418–29423.
13. Lin, S.; Xu, L.; Xu, C.; Chen, X.; Wang, A.; Zhang, B.; Lin, P.; Yang, Y.; Zhao, H.; Wang, Z. L. Electron Transfer in Nanoscale Contact Electrification: Effect of Temperature in the Metal-Dielectric Case. *Adv. Mater.* **2019,** *31,* 1808197.
14. Lin, S.; Xu, L.; Zhu, L.; Chen, X.; Wang, Z. L. Electron Transfer in Nanoscale Contact Electrification: Photon Excitation Effect. *Adv. Mater.* **2019,** *31,* 1901418.
15. Elsdon, R.; Mitchell, F. R. G. Contact Electrification of Polymers. *J. Phys. D. Appl. Phys.* **1976,** *9,* 1445–1460.
16. Lowell, J. Contact Electrification of Metals. *J. Phys. D. Appl. Phys.* **1975,** *8,* 53–63.
17. Sow, M.; Widenor, R.; Kumar, A.; Lee, S.; Lacks, D.; Sankaran, R. Strain-Induced Reversal of Charge Transfer in Contact Electrification. *Angew. Chem. Int. Ed.* **2012,** *124,* 2749–2751.
18. Zhang, Y.; Shao, T. Contact Electrification Between Polymers and Steel. *J. Electrostat.* **2013,** *71,* 862–866.
19. Harper, W. R. Contact Electrification of Semiconductors. *Br. J. Appl. Phys.* **1960,** *11,* 324–331.
20. Hays, D. A. Contact Electrification Between Mercury and Polyethylene: Effect of surface Oxidation. *J. Chem. Phys.* **1974,** *61,* 1455–1462.
21. Sosa, M. D.; Ricci, M. L. M.; Missoni, L. L.; Murgida, D. H.; Canneva, A.; D'Accorso, N. B.; Negri, R. M. Liquid-Polymer Triboelectricity: Chemical Mechanisms in the Contact Electrification Process. *Soft Matter* **2020,** *16,* 7040–7051.
22. Li, S.; Nie, J.; Shi, Y.; Tao, X.; Wang, F.; Tian, J.; Lin, S.; Chen, X.; Wang, Z. L. Contribution of Different Functional Groups to Contact Electrification of Polymers. *Adv. Mater.* **2020,** *32,* 2001307.
23. Nauruzbayeva, J.; Sun, Z.; Gallo, A.; Ibrahim, M.; Santamarina, J. C.; Mishra, H. Electrification at Water-Hydrophobe Interfaces. *Nat. Commun.* **2020,** *11,* 5285.
24. Nie, J.; Wang, Z.; Ren, Z.; Li, S.; Chen, X.; Wang, Z. L. Power Generation From the Interaction of a Liquid Droplet and a Liquid Membrane. *Nat. Commun.* **2019,** *10,* 2264.
25. Wang, P.; Zhang, S.; Zhang, L.; Wang, L.; Xue, H.; Wang, Z. L. Non-contact and Liquid-Liquid Interfacing Triboelectric Nanogenerator for Self-Powered Water/Liquid Level Sensing. *Nano Energ.* **2020,** *72,* 104703.
26. Jiang, P.; Zhang, L.; Guo, H.; Chen, C.; Wu, C.; Zhang, S.; Wang, Z. L. Signal Output of Triboelectric Nanogenerator at Oil-Water Solid Multiphase Interfaces and Its Application for Dual-Signal Chemical Sensing. *Adv. Mater.* **2019,** *31,* 1902793.
27. Zaera, F. Liquid/Solid Interfaces at the Molecular Level. *Chem. Rev.* **2012,** *112,* 2920–2986.
28. Magnussen, O. M.; Grob, A. Toward an Atomic-Scale Understanding of Electrochemical Interface Structure and Dynamics. *J. Am. Chem. Soc.* **2019,** *141,* 4777–4790.

29. Oja, S. M.; Wood, M.; Zhang, B. Nanoscale Electrochemistry. *Anal. Chem.* **2013,** *85,* 473–486.
30. Yuan, H.; Shimotani, H.; Ye, J.; Yoon, S.; Aliah, H.; Tsukazak, A.; Kawasaki, M.; Iwasa, Y. Electrostatic and Electrochemical Nature of Liquid-Gated Electric-Double-Layer Transistors Based on Oxide. *J. Am. Chem. Soc.* **2010,** *132,* 18402–18407.
31. Favaro, M.; Jeong, B.; Ross, P. N.; Yano, J.; Hussain, Z.; Liu, Z.; Crumlim, E. J. Unravelling the Electrochemical Double Layer by Direct Probing of the Solid/Liquid Interface. *Nat. Commun.* **2016,** *7*, 12695.
32. Strasser, P.; Gliech, M.; Kuehl, S.; Moeller, T. Electrochemical Processes on Solid Shaped Nanoparticles with Defined Facets. *Chem. Soc. Rev.* **2018,** *47,* 715–735.
33. Nedrygailov, I. I.; Lee, C.; Moon, S. Y.; Lee, H.; Park, J. Y. Hot Electrons at Solid-Liquid Interfaces: A Large Chemoelectric Effect During the Catalytic Decomposition of Hydrogen Peroxide. *Angew. Chem. Int. Ed.* **2016,** *55,* 10859–10862.
34. Kolmakov, A.; Moskovits, M. Chemical Sensing and Catalysis by One-Dimensional Metal-Oxide. *Annu. Rev. Mater. Res.* **2004,** *34,* 151–180.
35. Bourikas, K.; Korduils, C.; Lycourghiotis, A. The Role of the Liquid-Solid Interface in the Preparation of Supported Catalysts. *Catal. Rev.* **2006,** *48,* 363–444.
36. Lee, S. H.; Nedrygailov, I. I.; Oh, S.; Park, J. Y. Hot Electron Flux at Solid-Liquid Interfaces Probed with Pt/Si Catalytic Nanodiodes: Effect of pH During Decomposition of Hydrogen Peroxide. *Catal. Today* **2018,** *303,* 282–288.
37. Tao, F.; Crozier, P. A. Atomic-Scale Observations of Catalyst Structures Under Reaction Conditions and During Catalysis. *Chem. Rev.* **2016,** *116,* 3487–3539.
38. Li, X.; Tian, H.; Shao, J.; Ding, Y.; Chen, X.; Wang, L.; Lu, B. Decreasing the Saturated Contact Angle in Electrowetting-on-Dielectrics by Controlling the Charge Trapping at Liquid-Solid Interfaces. *Adv. Funct. Mater.* **2016,** *26,* 2994–3002.
39. Quinn, A.; Sedev, R.; Ralston, J. Contact Angle Saturation in Electrowetting. *J. Phys. Chem. B* **2005,** *109,* 6268–6275.
40. Pollack, M. G.; Shenderov, A. D.; Fair, R. B. Electrowetting-Based Actuation of Droplets for Integrated Microfluidics. *Lab. Chip* **2002,** *2,* 96–101.
41. Mugele, F.; Baret, J. Electrowetting: From Basis to Applications. *J. Phys. Condens. Matter* **2005,** *17,* 705–774.
42. Hierrezuelo, J.; Sadeghpour, A.; Szilagyi, I.; Vaccaro, A.; Borkovec, M. Electrostatic Stabilization of Charged Colloidal Particles with Adsorbed Polyelectrolytes of Opposite Charge. *Langmuir* **2010,** *26,* 15109–15111.
43. Crocker, J. C.; Grier, D. G. Microscopic Measurement of the Pair Interaction Potential of Charge-Stabilized Colloid. *Phys. Rev. Lett.* **1994,** *73,* 352–355.
44. Behrens, S. H.; Borkovee, M. Electrostatic Interaction of Colloidal Surfaces with Variable Charge. *J. Phys. Chem. B* **1999,** *103,* 2918–2928.
45. Liufu, S.; Xiao, H.; Li, Y. Adsorption of Poly (Acrylic Acid) Onto the Surface of Titanium Dioxide and the Colloidal Stability of Aqueous Suspension. *J. Colloid Interf. Sci.* **2005,** *281,* 155–163.
46. Copeland, A. W.; Black, O. D.; Garrett, A. B. The Photovoltaic Effect. *Chem. Rev.* **1942,** *31,* 177–226.
47. Williams, F.; Nozik, A. J. Solid-State Perspectives of the Photoelectrochemistry of Semiconductor-Electrolyte Junctions. *Nature* **1984,** *312,* 21–27.
48. Lewis, N. S. Progress in Understanding Electron-Transfer Reactions at Semiconductor/Liquid Interfaces. *J. Phys. Chem. B* **1998,** *102,* 4843–4855.
49. Iqbal, A.; Hossain, M. S.; Bevan, K. H. The Role of Relative Rate Constants in Determining Surface State Phenomena at Semiconductor-Liquid Interfaces. *Phys. Chem. Chem. Phys.* **2016,** *18,* 29466–29477.
50. Tachibana, Y.; Vayssieres, L.; Durrant, J. R. Artificial Photosynthesis for Solar Water-Splitting. *Nat. Photon.* **2012,** *6,* 5111–5518.
51. Mubeen, S.; Lee, J.; Singh, N.; Kramer, S.; Stucky, G. D.; Moskovits, M. An Autonomous Photosynthetic Device in Which all Charge Carriers Derive From Surface Plasmons. *Nat. Nanotechnol.* **2013,** *8,* 247–251.
52. Lewis, N. S. Developing a Scalable Artificial Photosynthesis Technology Through Nanomaterials by Design. *Nat. Nanotechnol.* **2016,** *11,* 1010–1019.
53. Tang, J.; Durrant, J. R.; Klug, D. R. Mechanism of Photocatalytic Water Splitting in $TiO_2$. Reaction of Water with Photoholes, Importance of Charge Carrier Dynamics, and Evidence for Four-Hole Chemistry. *J. Am. Chem. Soc.* **2008,** *130,* 13885–13891.
54. Wolcott, A.; Smith, W. A.; Kuykendall, T. R.; Zhao, Y.; Zhang, J. Z. Photoelectrochemical Water Splitting Using Dense and Aligned $TiO_2$ Nanorod Arrays. *Small* **2009,** *5,* 104–111.
55. Cowan, A. J.; Tang, J.; Leng, W.; Durrant, J. R.; Klug, D. R. Water Splitting by Nanocrystalline $TiO_2$ in a Complete Photoelectrochemical Cell Exhibits Efficiencies Limited by Charge Recombination. *J. Phys. Chem. C* **2010,** *114,* 4208–4214.
56. Wang, Z. L.; Wang, A. On the Origin of Contact-Electrification. *Mater. Today* **2019,** *30,* 34–51.
57. Schmickler, W. Electronic Effects in the Electric Double Layer. *Chem. Rev.* **1996,** *96,* 3177–3200.
58. Jiang, D.; Wu, J. Microscopic Insights Into the Electrochemical Behavior of Nonaqueous Electrolytes in Electric Double Layer Capacitors. *J. Phys. Chem. Lett.* **2013,** *4,* 1260–1267.
59. Liu, H.; Steigerwald, M. L.; Nuckolls, C. Electrical Double Layer Catalyzed Wet-Etching of Silicon Dioxide. *J. Am. Chem. Soc.* **2009,** *131,* 17034–17035.
60. Dijkstra, M.; Hansen, J. P.; Madden, P. A. Gelation of a Clay Colloid Suspension. *Phys. Rev. Lett.* **1995,** *75,* 2236–2239.
61. Lopez-Garcia, J. J.; Aranda-Rascon, M. J.; Horno, J. Electrical Double Layer Around a Spherical Colloid Particle: The Excluded Volume Effect. *J. Coll. Interf. Sci.* **2007,** *316,* 196–201.
62. Simon, P.; Gogotsi, Y. Materials for Electrochemical Capacitors. *Nat. Mater.* **2008,** *7*, 1476-1122.
63. Trefalt, G.; Behrens, S. H.; Borkovec, M. Charge Regulation in the Electrical Double Layer: Ion Adsorption and Surface Interactions. *Langmuir* **2015,** *32,* 380–400.
64. Liu, H.; Vecitis, C. D. Reactive Transport Mechanism for Organic Oxidation During Electrochemical Filtration: Mass-Transfer, Physical Adsorption, and Electron-Transfer. *J. Phys. Chem. C* **2011,** *116,* 374–383.
65. Marcus, R. A. Chemical and Electrochemical Electron-Transfer Theory. *Annu. Rev. Phys. Chem.* **1964,** *15,* 155–196.
66. Marcus, R. A. On the Theory of Oxidation-Reduction Reactions of Electrochemical and Chemical Rate Constants. *J. Phys. Chem.* **1963,** *67,* 853–857.
67. Predota, M.; Bandura, A. V.; Cummings, P. T.; Kubicki, J. D.; Wesolowski, D. J.; Chialvo, A. A.; Machesky, M. L. Electric Double Layer at The Rutile (110) Surface. 1. Structure of Surfaces and Interfacial Water From Molecular Dynamics by Use of Ab Initio Potentials. *J. Phys. Chem. B* **2004,** *108,* 12049–12060.
68. Sakong, S.; Grob, A. The Electric Double Layer at Metal-Water Interfaces Revisited Based on a Charge Polarization Scheme. *J. Chem. Phys.* **2018,** *149*, 084705.
69. Outhwaite, C. W.; Bhuiyan, L. B. An Improved Modified Poisson-Boltzmann Equation in Electric-Double-Layer Theory. *J. Chem. Soc. Faraday Trans.* **1983,** *79,* 707–718.
70. Lowell, J. Surface States and the Contact Electrification of Polymers. *J. Phys. D. Appl. Phys.* **1977,** *10,* 65–71.
71. Wiles, J.; Fialkowski, M.; Radowski, M.; Whitesides, G. M. Effects of Surface Modification and Moisture on the Rates of Charge Transfer Between Metals and Organic Materials. *J. Phys. Chem. B* **2004,** *108,* 20296–20302.
72. Byun, K.; Cho, Y.; Seo, M.; Kim, S.; Kim, S.; Shin, H.; Park, S.; Hwang, S. Control of Triboelectrification by Engineering Surface Dipole and Surface Electronic State. *ACS Appl. Mater. Inter.* **2016,** *8,* 18519–18525.
73. Angus, J. C.; Greber, I. Tribo-electric Charging of Dielectric Solids of Identical Composition. *J. Appl. Phys.* **2018,** *123*, 174102.
74. Pence, S.; Novotny, V.; Diaz, A. Effect of Surface Moisture on Contact Charge of Polymers Containing Ions. *Langmuir* **1994,** *10,* 592–596.
75. Lowell, J.; Rose-Innes, A. Contact Electrification. *Adv. Phys.* **1980,** *29,* 947–1023.
76. El-Kazzaz, A.; Rose-Innes, A. C. Contact Charging of Insulators by Liquid Metals. *J. Electrostat.* **1985,** *16,* 157–163.
77. Matsui, M.; Murasaki, N.; Fujibayashi, K.; Bao, P. Y.; Kishimoto, Y. Electrification of Pure Water Flowing Down a Trough Set Up with a Resin Sheet. *J. Electrostat.* **1993,** *31,* 1–10.
78. Yatsuzuka, K.; Mizuno, Y.; Asano, K. Electrification Phenomena of Pure Water Droplets Dripping and Sliding on a Polymer Surface. *J. Electrostat.* **1994,** *32,* 157–171.
79. Yatsuzuka, K.; Higashiyama, Y.; Asano, K. Electrification of Polymer Surface Caused by Sliding Ultrapure Water. *IEEE T. Ind. Appl.* **1996,** *32,* 825–831.
80. Burgo, T.; Galembeck, F.; Pollack, G. H. Where is Water in the Triboelectric Series? *J. Electrostat.* **2016,** *80,* 30–33.
81. Zhang, Y.; Pahtz, T.; Liu, Y.; Wang, X.; Zhang, R.; Shen, Y.; Ji, R.; Cai, B. Electric Field and Humidity Trigger Contact Electrification. *Phys. Rev. X* **2015,** *5*, 011002.
82. Diaz, A. F. Contact Electrification of Materials: the Chemistry of Ions on Polymer Surfaces. *J. Adhes.* **1998,** *67,* 111–122.

83. Lin, Z.; Cheng, G.; Lee, S.; Pradel, K.; Wang, Z. L. Harvesting Water Drop Energy by a Sequential Contact-Electrification and Electrostatic-Induction Process. *Adv. Mater.* **2014,** *26,* 4690–4696.
84. Liu, X.; Cheng, K.; Cui, P.; Qi, H.; Qin, H.; Gu, G.; Shang, W.; Wang, S.; Cheng, G.; Du, Z. Hybrid Energy Harvester with Bi-Functional Nano-Wrinkled Anti-reflective PDMS Film for Enhancing Energies Conversion From Sunlight and Raindrops. *Nano Energ.* **2019,** *66*, 104188.
85. Cheng, G.; Lin, Z.; Du, Z.; Wang, Z. L. Simultaneously Harvesting Electrostatic and Mechanical Energies From Flowing Water by a Hybridized Triboelectric Nanogenerator. *ACS Nano* **2014,** *8,* 1932–1939.
86. Zhu, G.; Su, Y.; Bai, P.; Chen, J.; Jing, Q.; Yang, W.; Wang, Z. L. Harvesting Water Wave Energy by Asymmetric Screening of Electrostatic Charges on a Nanostructured Hydrophobic Thin-Film Surface. *ACS Nano* **2014,** *8,* 6031–6037.
87. Pan, L.; Wang, J.; Wang, P.; Gao, R.; Wang, Y.; Zhang, X.; Zou, J.; Wang, Z. L. Liquid-FEP-Based U-Tube Triboelectric Nanogenerator for Harvesting Water-Wave Energy. *Nano Res.* **2018,** *11,* 4062–4073.
88. Li, X.; Tao, J.; Wang, X.; Zhu, J.; Pan, C.; Wang, Z. L. Networks of High Performance Triboelectric Nanogenerators Based on Liquid-Solid Interface Contact Electrification for Harvesting Low-Frequency Blue Energy. *Adv. Energ. Mater.* **2018,** *8,* 1800705.
89. Le, C.; Vo, C.; Nguyen, T.; Vu, D.; Ahn, K. Liquid-Solid Contact Electrification Based on Discontinuous-Conduction Triboelectric Nanogenerator Induced by Radially Symmetrical Structure. *Nano Energ.* **2021,** *80*, 105571.
90. Xu, M.; Wang, S.; Zhang, S.; Ding, W.; Kien, P.; Wang, C.; Li, Z.; Pan, X.; Wang, Z. L. A Highly-Sensitive Wave Sensor Based on Liquid-Solid Interfacing Triboelectric Nanogenerator for Smart Marine Equipment. *Nano Energ.* **2019,** *57,* 574–580.
91. Cho, H.; Chung, J.; Shin, G.; Sim, J.; Kim, D.; Lee, S.; Hwang, W. Toward Sustainable Output Generation of Liquid-Solid Contact Triboelectric Nanogenerators: The Role of Hierarchical Structures. *Nano Energ.* **2019,** *56,* 56–64.
92. Lin, Z.; Cheng, G.; Lin, L.; Lee, S.; Wang, Z. L. Water-Solid Surface Contact Electrification and Its Use for Harvesting Liquid-Wave Energy. *Angew. Chem. Int. Ed.* **2013,** *52,* 12545–12549.
93. Yang, X.; Chan, S.; Wang, L.; Daoud, W. Water Tank Triboelectric Nanogenerator for Efficient Harvesting of Water Wave Energy Over a Broad Frequency Range. *Nano Energ.* **2018,** *44,* 388–398.
94. Ha, J.; Chung, J.; Kim, S.; Kim, J.; Shin, S.; Park, J.; Lee, S.; Kim, J. Transfer-Printable Micropatterned Fluoropolymer-Based Triboelectric Nanogenerator. *Nano Energ.* **2017,** *36,* 126–133.
95. Lin, S.; Xu, L.; Wang, A.; Wang, Z. L. Quantifying Electron-Transfer in Liquid-Solid Contact Electrification and the Formation of Electric Double-Layer. *Nat. Commun.* **2020,** *11,* 399.
96. Nie, J.; Ren, Z.; Xu, L.; Lin, S.; Zhan, F.; Chen, X.; Wang, Z. L. Probing Contact-Electrification-Induced Electron and Ion Transfers at Liquid-Solid Interface. *Adv. Mater.* **2019,** *32*, 1905696.
97. Zhan, F.; Wang, A.; Xu, L.; Lin, S.; Shao, J.; Chen, X.; Wang, Z. L. Electron Transfer as a Liquid Droplet Contacting a Polymer Surface. *ACS Nano* **2020,** *14,* 17565–17573.
98. Xu, C.; Zi, Y.; Wang, A.; Zou, H.; Dai, Y.; He, X.; Wang, P.; Wang, Y.; Feng, P.; Li, D.; Wang, Z. L. On the Electron-Transfer Mechanism in the Contact-Electrification Effect. *Adv. Mater.* **2018,** *30*, 1706790.
99. Helmholtz, H. Ober Einige Gesetzeder Verberitung Elektrischer Strijime in Kdperlichen Leitern Mit Anwendung auf Die Theorischelektrischen Versuche. *Ann. Phys. Chem.* **1853,** *89,* 21–33.
100. Gouy, M. Sur La Constitution De La Charge Electrique a La Surface D'Un Electrolyte. *J. Phys. Theor. Appl.* **1910,** *9,* 457–468.
101. Chapman, D. L. A Contribution to the Theory of Electrocapillarity. *Philos. Mag.* **1913,** *25,* 475–481.
102. Stern, O. The Theory of the Electric Double Layer. *Electrochem* **1924,** *30,* 508.
103. Zhang, L. L.; Zhao, X. S. Carbon-Based Materials as Supercapacitor Electrodes. *Chem. Soc. Rev.* **2009,** *38,* 2520–2531.
104. Stamenkovic, V. R.; Strmcnik, D.; Lopes, P. P.; Markovic, N. M. Energy and Fuels From Electrochemical Interfaces. *Nat. Mater.* **2017,** *16,* 57–69.
105. Wu, T.; Wang, G.; Dong, Q.; Zhan, F.; Zhang, X.; Li, S.; Qiao, H.; Qiu, J. Starch Derived Porous Carbon Nanosheets for High Performance Photovoltaic Capacitive Deionization. *Environ. Sci. Technol.* **2017,** *51,* 9244–9251.
106. Srimuk, P.; Su, X.; Yoon, J.; Aurbach, D.; Presser, V. Charge Transfer Materials for Electrochemical Water Desalination, Ion Separation and the Recovery of Elements. *Nat. Rev. Mater.* **2020,** *5,* 517–538.
107. Du, H.; Lin, X.; Xu, Z.; Chu, D. Electric Double-Layer Transistors: A Review of Recent Progress. *J. Mater. Sci.* **2015,** *50,* 5641–5673.
108. Mark, D.; Haeberle, S.; Roth, G.; von Stetten, F.; Zengerle, R. Microfluidic Lab-on-a-Chip Platforms: Requirements, Characteristics and Applications. *Chem. Soc. Rev.* **2010,** *39,* 1153–1182.
109. Quinn, A.; Sedev, R.; Ralston, J. Influence of the Electrical Double Layer in Electrowetting. *J. Phys. Chem. B* **2003,** *107,* 1163–1169.
110. Liang, Y.; Hilal, N.; Langston, P.; Starov, V. Interaction Forces Between Colloidal Particles in Liquid: Theory and Experiment. *Adv. Colloid Interf. Sci.* **2007,** *134–135,* 151–166.
111. Zhan, F.; Wang, G.; Wu, T. T.; Dong, Q.; Meng, Y. L.; Wang, J. R.; Yang, J.; Li, S. F.; Qiu, J. S. High Performance Asymmetric Capacitive Mixing with Oppositely Charged Carbon Electrodes for Energy Production From Salinity Differences. *J. Mater. Chem. A* **2017,** *5,* 20374–20380.
112. Zhan, F.; Wang, Z. J.; Wu, T. T.; Dong, Q.; Zhao, C. T.; Wang, G.; Qiu, J. S. High Performance Concentration Capacitors with Graphene Hydrogel Electrodes for Harvesting Salinity Gradient Energy. *J. Mater. Chem. A* **2018,** *6,* 4981–4987.
113. Raiteri, R.; Martinoia, S.; Grattarola, M. pH-Dependent Charge Density at the Insulator-Electrolyte Interface Probed by a Scanning Force Microscope. *Biosens. Bioelectron.* **1996,** *11,* 1009–1017.
114. Davis, J.; James, R.; Leckie, J. Surface Ionization and Complexation at Oxide-Water Interface. 1. Computation of Electrical Double-Layer Properties in Simple Electrolytes. *J. Colloid Interf. Sci.* **1978,** *63,* 480–499.
115. Lagstrom, T.; Gmur, T.; Quaroni, L.; Goel, A.; Brown, M. Surface Vibrational Structure of Colloidal Silica and Its Direct Correlation with Surface Charge Density. *Langmuir* **2015,** *31,* 3621–3626.
116. Bousse, L.; Rooij, N.; Bergveld, P. Operation of Chemically Sensitive Field-Effect Sensors as a Function of the Insulator-Electrolyte Interface. *IEEE T. Electron. Dev.* **1983,** *30,* 1263–1270.
117. Gmur, T.; Goel, A.; Brown, M. Quantifying Specific Ion Effects on the Surface Potential and Charge Density at Silica Nanoparticle-Aqueous Electrolyte Interfaces. *J. Phys. Chem. C* **2016,** *120,* 16617–16625.
118. Burg, K.; Delahay, P. Photoelectron Emission Spectroscopy of Inorganic Anions in Aqueous Solution. *Chem. Phys. Lett.* **1981,** *78,* 287–290.
119. Takakuwa, Y.; Niwano, M.; Nogawa, M.; Katakura, H.; Matsuyoshi, S.; Ishida, H. Photon-Stimulated Desorption of $H^+$ Ions From Oxidized Si(111) Surfaces. *Jpn. J. Appl. Phys.* **1989,** *28,* 2581–2586.
120. Vácha, R.; Zangi, R.; Engberts, J. B. F. N.; Jungwirth, P. Water Structuring and Hydroxide Ion Binding at the Interface Between Water and Hydrophobic Walls of Varying Rigidity and Van Der Waals Interactions. *J. Phys. Chem. C* **2008,** *112,* 7689–7692.
121. Dicke, C.; Hähner, G. Interaction Between a Hydrophobic Probe and Tri(ethylene glycol)-Containing Self-Assembled Monolayers on Gold Studied with Force Spectroscopy in Aqueous Electrolyte Solution. *J. Phys. Chem. B* **2002,** *106,* 4450–4456.
122. Dreher, W.; Leibfritz, D. New Method for the Simultaneous Detection of Metabolites and Water in Localized In Vivo $^1$H Nuclear Magnetic Resonance Spectroscopy. *Magn. Reson. Med.* **2005,** *54,* 190–195.
123. Tang, W.; Jiang, T.; Fan, F. R.; Yu, A. F.; Zhang, C.; Cao, X.; Wang, Z. L. Liquid-Metal Electrode for High-Performance Triboelectric Nanogenerator at an Instantaneous Energy Conversion Efficiency of 70.6%. *Adv. Funct. Mater.* **2015,** *25,* 3718–3725.

124. Zou, H.; Zhang, Y.; Guo, L.; Wang, P.; He, X.; Dai, G.; Zheng, H.; Chen, C.; Wang, A. C.; Xu, C.; Wang, Z. L. Quantifying the Triboelectric Series. *Nat. Commun.* **2019,** *10,* 1427.
125. Niu, S.; Liu, Y.; Wang, S.; Lin, L.; Zhou, Y. S.; Hu, Y.; Wang, Z. L. Theoretical Investigation and Structural Optimization of Single-Electrode Triboelectric Nanogenerators. *Adv. Funct. Mater.* **2014,** *24,* 3332–3340.
126. Wu, H.; Mendel, N.; van den Ende, D.; Zhou, G.; Mugele, F. Energy Harvesting From Drops Impacting Onto Charged Surfaces. *Phys. Rev. Lett.* **2020,** *125*, 078301.
127. Niu, S.; Liu, Y.; Chen, X.; Wang, S.; Zhou, Y. S.; Lin, L.; Xie, Y.; Wang, Z. L. Theory of Freestanding Triboelectric-Layer-Based Nanogenerators. *Nano Energ.* **2015,** *12,* 760–774.
128. Willatzen, M.; Voon, L.; Wang, Z. L. Quantum Theory of Contact Electrification for Fluids and Solids. *Adv. Funct. Mater.* **2020,** *30*, 1910461.
129. Li, L.; Wqang, X.; Zhu, P.; Li, H.; Wang, F.; Wu, J. The Electron Transfer Mechanism Between Metal and Amorphous Polymers in Humidity Environment for Triboelectric Nanogenerator. *Nano Energ.* **2020,** *70,* 104476.
130. Sun, M.; Lu, Q.; Wang, Z. L.; Huang, B. Understanding Contact Electrification at Liquid-Solid Interfaces From Surface Electronic Structure. *Nat. Commun.* **2021,** *12,* 1752.
131. Lin, S.; Shen, R.; Yao, T.; Lu, Y.; Feng, S.; Hao, Z.; Zheng, H.; Yan, Y.; Li, E. Surface States Enhanced Dynamic Schottky Diode Generator with Extremely High-Power Density Over 1000 W $m^{-2}$. *Adv. Sci.* **2019,** *6*, 1901925.
132. Zhang, Z.; Jiang, D.; Zhao, J.; Liu, G.; Bu, T.; Zhang, C.; Wang, Z. L. Tribovoltaic Effect on Metal–Semiconductor Interface for Direct-Current Low-Impedance Triboelectric Nanogenerators. *Adv. Energ. Mater.* **2020,** *10,* 1–8.
133. Liu, J.; Miao, M.; Jiang, K.; Khan, F.; Goswami, A.; McGee, R.; Li, Z.; Nguyen, L.; Hu, Z.; Lee, J.; Cadien, K.; Thundat, T. Sustained Electron Tunneling at Unbiased Metal-Insulator-Semiconductor Triboelectric Contacts. *Nano Energ.* **2018,** *48,* 320–326.
134. Williams, F.; Varma, S. P.; Hillenius, S. Liquid Water as a Long-Pair Amorphous Semiconductor. *J. Chem. Phys.* **1976,** *64,* 1549–1554.
135. Lin, S.; Chen, X.; Wang, Z. L. The Tribovoltaic Effect and Electron Transfer at a Liquid-Semiconductor Interface. *Nano Energ.* **2020,** *76*, 105070.
136. Zheng, M.; Lin, S.; Tang, Z.; Feng, Y.; Wang, Z. L. Photovoltaic Effect and Tribovoltaic Effect at Liquid-Semiconductor Interface. *Nano Energ.* **2021,** *83*, 105810.
137. Zheng, M.; Lin, S.; Xu, L.; Zhu, L.; Wang, Z. L. Scanning Probing of the Tribovoltaic Effect at the Sliding Interface of Two Semiconductors. *Adv. Mater.* **2020,** *32,* 2000928.
138. Le, J.; Fan, Q.; Perez-Martinez, L.; Cuesta, A.; Cheng, J. Theoretical Insight Into the Vibrational Spectra of Metal-Water Interfaces From Density Functional Theory Based Molecular Dynamics. *Phys. Chem. Chem. Phys.* **2018,** *20*, 11554.
139. Lin, S.; Xu, C.; Xu, L.; Wang, Z. L. The Overlapped Electron-Cloud Model for Electron Transfer in Contact Electrification. *Adv. Funct. Mater.* **2020,** *30*, 1909724.
140. Willatzen, M.; Wang, Z. L. Theory of Contact Electrification: Optical Transitions in Two-Level Systems. *Nano Energ.* **2018,** *52,* 517–523.
141. Snyder, G. J.; Toberer, E. S. Complex Thermoelectric Materials. *Nat. Mater.* **2008,** *7,* 105–114.
142. Dudem, B.; Huynh, N. D.; Kim, W.; Kim, D. H.; Hwang, H. J.; Choi, D.; Yu, J. S. Nanopillar-Array Architectured PDMS-Based Triboelectric Nanogenerator Integrated with a Windmill Model for Effective Wind Energy Harvesting. *Nano Energ.* **2017,** *42,* 269–281.
143. Lee, J. H.; Kim, S.; Kim, T. Y.; Khan, U.; Kim, S. W. Water Droplet-Driven Triboelectric Nanogenerator with Superhydrophobic Surface. *Nano Energ.* **2019,** *58,* 579–584.
144. Kwak, S. S.; Lin, S.; Lee, J. H.; Ryu, H.; Kim, T. Y.; Zhong, H.; Chen, H.; Kim, S. W. Triboelectrification-Induced Large Electric Power Generation From a Single Moving Droplet on Graphene/Polytetrafluoroethylene. *ACS Nano* **2016,** *10,* 7297–7302.
145. Xu, W.; Zheng, H.; Liu, Y.; Zhou, X.; Zhang, C.; Song, Y.; Deng, X.; Leung, M.; Yang, Z.; Xu, R.; Wang, Z. L.; Zeng, X. C.; Wang, Z. A Droplet-Based Electricity Generator with High Instantaneous Power Density. *Nature* **2020,** *578,* 392–396.
146. Liang, Q.; Yan, X.; Liao, X.; Zhang, Y. Integrated Multi-unit Transparent Triboelectric Nanogenerator Harvesting Rain Power for Driving Electronics. *Nano Energ.* **2016,** *25,* 18–25.
147. Choi, D.; Kim, D. W.; Yoo, D.; Cha, K. J.; La, M.; Kim, D. S. Spontaneous Occurrence of Liquid-Solid Contact Electrification in Nature: Toward a Robust Triboelectric Nanogenerator Inspired by the Natural Lotus Leaf. *Nano Energ.* **2017,** *36,* 250–259.
148. Zhao, L.; Liu, L.; Yang, X.; Hong, H.; Yang, Q.; Wang, J.; Tang, Q. Cumulative Charging Behavior of Water Droplet Driven Freestanding Triboelectric Nanogenerators Toward Hydrodynamic Energy Harvesting. *J. Mater. Chem. A* **2020,** *8,* 7880–7888.
149. Xiong, J.; Kin, M.; Wang, J.; Gaw, S.; Parida, K.; Lee, P. Wearable All-Fabric-Based Triboelectric Generator for Water Energy Harvesting. *Adv. Energ. Mater.* **2017,** *7*, 1701243.
150. Zhang, L.; Zhang, N.; Yang, Y.; Xiang, S.; Tao, C.; Yang, S.; Fan, X. Self-Powered All-in-One Fluid Sensor Textile with Enhanced Triboelectric Effect on All-Immersed Dendritic Liquid-Solid Interface. *ACS Appl. Mater. Inter.* **2018,** *10,* 30819–30826.
151. Yang, D.; Ni, Y.; Su, H.; Shi, Y.; Liu, Q.; Chen, X.; He, D. Hybrid Energy System Based on Solar Cell and Self-Healing/Self-Cleaning Triboelectric Nanogenerator. *Nano Energ.* **2021,** *79,* 105394.
152. Zheng, L.; Cheng, G.; Chen, J.; Lin, L.; Wang, J.; Liu, Y.; Li, H.; Wang, Z. L. A Hybridized Power Panel to Simultaneously Generate Electricity From Sunlight, Raindrops, and Wind Around the Clock. *Adv. Energ. Mater.* **2015,** *5*, 1501152.
153. Ren, Z.; Ding, Y.; Nie, J.; Wang, F.; Xu, L.; Lin, S.; Chen, X.; Wang, Z. L. Environmental Energy Harvesting Adapting to Different Weather Conditions and Self-Powered Vapor Sensor Based on Humidity-Responsive Triboelectric Nanogenerators. *ACS Appl. Mater. Inter.* **2019,** *11,* 6143–6153.
154. Jiang, D.; Su, Y.; Wang, K.; Wang, Y.; Xu, M.; Dong, M.; Chen, G. A Triboelectric and Pyroelectric Hybrid Energy Harvester for Recovering Energy From Low-Grade Waste Fluids. *Nano Energ.* **2020,** *70*, 104459.
155. Xu, W.; Wang, Z. Fusion of Slippery Interfaces and Transistor-Inspired Architecture for Water Kinetic Energy Harvesting. *Joule* **2020,** *4,* 1–5.
156. Xu, W.; Zhou, X.; Hao, C.; Zheng, H.; Liu, Y.; Yan, X.; Yang, Z.; Leung, M.; Zeng, X.; Xu, R.; Wang, Z. SLIPS-TENG: Robust Triboelectric Nanogenerator with Optical and Charge Transparency Using a Slippery Interface. *Natl. Sci. Rev.* **2019,** *6,* 540–550.
157. Zhong, W.; Xu, L.; Zhan, F.; Wang, H.; Wang, F.; Wang, Z. L. Dripping Channel Based Liquid Triboelectric Nanogenerators for Energy Harvesting and Sensing. *ACS Nano* **2020,** *14,* 10510–10517.
158. Lee, J.; Hwang, W. Theoretical Study of Micro/Nano Roughness Effect on Water-Solid Triboelectrification with Experimental Approach. *Nano Energ.* **2018,** *52,* 315–322.
159. Helseth, L. E. The Influence of Microscale Surface Roughness on Water-Droplet Contact Electrification. *Langmuir* **2019,** *35,* 8268–8275.
160. Wang, S.; Xie, Y.; Niu, S.; Lin, L.; Liu, C.; Zhou, Y.; Wang, Z. L. Maximum Surface Charge Density for Triboelectric Nanogenerators Achieved by Ionized-Air Injection: Methodology and Theoretical Understanding. *Adv. Mater.* **2014,** *26,* 6720–6728.
161. Jang, S.; La, M.; Cho, S.; Yun, Y.; Choi, J.; Ra, Y.; Park, S.; Choi, D. Monocharged Electret Based Liquid-Solid Interacting Triboelectric Nanogenerator for Its Boosted Electrical Output Performance. *Nano Energ.* **2020,** *70*, 104541.
162. Yoo, D.; Park, S.-C.; Lee, S.; Sim, J.-Y.; Song, I.; Choi, D.; Lim, H.; Kim, D. S. Biomimetic Anti-reflective Triboelectric Nanogenerator for Concurrent Harvesting of Solar and Raindrop Energies. *Nano Energ.* **2019,** *57,* 424–431.
163. Zhang, R.; Wang, S.; Yeh, M.; Pan, C.; Lin, L.; Yu, R.; Zhang, Y.; Zheng, L.; Jiao, Z.; Wang, Z. L. A Streaming Potential/Current-Based Microfluidic Direct Current Generator for Self-Powered Nanosystems. *Adv. Mater.* **2015,** *27,* 6482–6487.
164. Cavusoglu, A.; Chen, X.; Gentine, P.; Sahin, O. Potential for Natural Evaporation as a Reliable Renewable Energy Resource. *Nat. Commun.* **2017,** *8,* 617.
165. Zhao, L.; Duan, J.; Liu, L.; Wang, J.; Duan, Y.; Vaillant-Roca, L.; Yang, X.; Tang, Q. Boosting Power Conversion Efficiency by Hybrid Triboelectric Nanogenerator/Silicon Tandem Solar Cell Toward Rain Energy Harvesting. *Nano Energ.* **2021,** *82*, 105773.
166. Shi, Q.; Wang, H.; Wang, T.; Lee, C. Self-Powered Liquid Triboelectric Microfluidic Sensor for Pressure Sensing and Finger Motion Monitoring Applications. *Nano Energ.* **2016,** *30,* 450–459.
167. Zou, Y.; Tan, P.; Shi, B.; Ouyang, H.; Jiang, D.; Liu, Z.; Li, H.; Yu, M.; Wang, C.; Qu, X.; et al. A Bionic Stretchable Nanogenerator for Underwater Sensing and Energy Harvesting. *Nat. Commun.* **2019,** *10,* 2695.

168. Chen, B. D.; Tang, W.; He, C.; Jiang, T.; Xu, L.; Zhu, L. P.; Gu, G. Q.; Chen, J.; Shao, J. J.; Luo, J. J.; et al. Ultrafine Capillary-Tube Triboelectric Nanogenerator as Active Sensor for Microliquid Biological and Chemical Sensing. *Adv. Mater. Technol.* **2018,** *3*, 1700229.
169. Nie, J.; Ren, Z.; Shao, J.; Deng, C.; Xu, L.; Chen, X.; Li, M.; Wang, Z. L. Self-Powered Microfluidic Transport System Based on Triboelectric Nanogenerator and Electrowetting Technique. *ACS Nano* **2018,** *12,* 1491–1499.
170. Chen, G.; Liu, X.; Li, S.; Dong, M.; Jiang, D. A Droplet Energy Harvesting and Actuation System for Self-Powered Digital Microfluidics. *Lab. Chip* **2018,** *18,* 1026–1034.
171. Zhu, H. R.; Tang, W.; Gao, C. Z.; Han, Y.; Li, T.; Cao, X.; Wang, Z. L. Self-Powered Metal Surface Anti-Corrosion Protection Using Energy Harvested From Rain Drops and Wind. *Nano Energy* **2015,** *14,* 193–200.
172. Zhao, X. J.; Zhu, G.; Fan, Y. J.; Li, H. Y.; Wang, Z. L. Triboelectric Charging at the Nanostructured Solid/Liquid Interface for Area-Scalable Wave Energy Conversion and Its Use in Corrosion Protection. *ACS Nano* **2015,** *9,* 7671–7677.
173. Loh, Z. H.; Doumy, G.; Arnold, C.; Kjellsson, L.; Southworth, S. H.; Haddad, A.; Kumagai, Y.; Tu, M. F.; Ho, P. J.; March, A. M.; Schaller, R. D.; Yusof, M. S.; Debnath, T.; Simon, M.; Welsch, R.; Inhester, L.; Khalili, K.; Nanda, K.; Krylov, A. I.; Moeller, S.; Coslovich, G.; Koralek, J.; Minitti, M. P.; Schlotter, W. F.; Rubensson, J. E.; Santra, R.; Young, L. Observation of the Fastest Chemical Processes in the Radiolysis of Water. *Science* **2020,** *367,* 179–182.
174. Gauduel, Y.; Pommeret, S.; Migus, A.; Antonetti, A. Some Evidence of Ultrafast $H2O^{+}$-Water Molecule Reaction in Femtosecond Photoionization of Pure Liquid Water: Influence on Geminate Pair Recombination Dynamics. *Chem. Phys.* **1990,** *149,* 1–10.
175. Lin, S.; Zheng, M.; Luo, J.; Wang, Z. L. Effects of Surface Functional Groups on Electron Transfer at Liquid–Solid Interfacial Contact Electrification. *ACS Nano* **2020,** *14,* 10733–10741.
176. Boswell, B. R.; Mansson, C. M. F.; Cox, J. M.; Jin, Z.; Romaniuk, J. A. H.; Lindquist, K. P.; Cegelski, L.; Xia, Y.; Lopez, S. A.; Burns, N. Z. Mechanochemical Synthesis of an Elusive Fluorinated Polyacetylene. *Nat. Chem.* **2021,** *13,* 41–46.
177. Adamczyk, Z.; Warszyński, P. Role of Electrostatic Interactions in Particle Adsorption. *Adv. Colloid Interf. Sci.* **1996,** *63,* 41–149.
178. Zhao, K.; He, K. Dielectric Relaxation of Suspensions of Nanoscale Particles Surrounded by a Thick Electric Double Layer. *Phys. Rev. B* **2006,** *74*, 205319.
179. Gao, G.; Wan, B.; Liu, X.; Sun, Q.; Yang, X.; Wang, L.; Pan, C.; Wang, Z. L. Tunable Tribotronic Dual-Gate Logic Devices Based on 2D $MoS_2$ and Black Phosphorus. *Adv. Mater.* **2018,** *30*, 1705088.
180. Poortinga, A. T.; Bos, R.; Norde, W.; Busscher, H. J. Electric Double Layer Interactions in Bacterial Adhesion to Surfaces. *Surf. Sci. Rep.* **2002,** *47,* 1–32.
181. Meng, Y.; Zhao, J.; Yang, X.; Zhao, C.; Qin, S.; Cho, J. H.; Zhang, C.; Sun, Q.; Wang, Z. L. Mechanosensation-Active Matrix Based on Direct-Contact Tribotronic Planar Graphene Transistor Array. *ACS Nano* **2018,** *12,* 9381–9389.
182. Israelachvili, J. *Intermolecular and Surface Forces*, University of California: Santa Barbara, California, USA, 2011.
183. Xia, M.; Nie, J.; Zhang, Z.; Lu, X.; Wang, Z. L. Suppressing Self-Discharge of Supercapacitors via Electrorheological Effect of Liquid Crystals. *Nano Energy* **2018,** *47,* 43–50.
184. Li, G.; Chuang, P.-Y. A. Identifying the Forefront of Electrocatalytic Oxygen Evolution Reaction: Electronic Double Layer. *Appl. Catal. B Environ.* **2018,** *239,* 425–432.
185. Liu, M.; Pang, Y.; Zhang, B.; De Luna, P.; Voznyy, O.; Xu, J.; Zheng, X.; Dinh, C. T.; Fan, F.; Cao, C.; et al. Enhanced Electrocatalytic $CO_2$ Reduction via Field-Induced Reagent Concentration. *Nature* **2016,** *537,* 382.
186. Ringe, S.; Clark, E. L.; Resasco, J.; Walton, A.; Seger, B.; Bell, A. T.; Chan, K. Understanding Cation Effects in Electrochemical $CO_2$ Reduction. *Energ. Environ. Sci.* **2019,** *12,* 3001–3014.
187. Otto, K.; Elwing, H.; Hermansson, M. The Role of Type 1 Fimbriae in Adhesion of *Escherichia coli* to Hydrophilic and Hydrophobic Surfaces. *Colloid Surf. B* **1999,** *15,* 99.
188. Fujimoto, T.; Awaga, K. Electric-Double-Layer Field-Effect Transistors with Ionic Liquids. *Phys. Chem. Chem. Phys.* **2013,** *15,* 8983–9006.
189. Daiguji, H.; Oka, Y.; Adachi, T.; Shirono, K. Theoretical Study on the Efficiency of Nanofluidic Batteries. *Electrrochem. Commun.* **2006,** *8,* 1796–1800.
190. Heyden, F.; Stein, D.; Dekker, C. Streaming Current in a Single Nanofluidic Channel. *Phys. Rev. Lett.* **2005,** *95*, 116104.
191. Zhu, Y.; Zhan, K.; Hou, X. Interface Design of Nanochannels for Energy Utilization. *ACS Nano* **2018,** *12,* 908–911.
192. Yin, J.; Li, X.; Yu, J.; Zhang, Z.; Zhou, J.; Guo, W. Generating Electricity by Moving a Droplet of Ionic Liquid Along Graphene. *Nat. Nanotechnol.* **2014,** *9,* 378–383.
193. Fan, B.; Bhattacharya, A.; Bandaru, P. Enhanced Voltage Generation Through Electrolyte Flow on Liquid-Filled Surfaces. *Nat. Commun.* **2018,** *9,* 4050.
194. Haldrup, S.; Catalano, J.; Hinge, M.; Jensen, G. V.; Pedersen, J. S.; Bentien, A. Tailoring Membrane Nanostructure and Charge Density for High Electrokinetic Energy Conversion Efficiency. *ACS Nano* **2016,** *10,* 2415–2423.
195. Zhang, J.; Zhan, K.; Wang, S.; Hou, X. Soft Interface Design for Electrokinetic Energy Conversion. *Soft Matter* **2020,** *16,* 2915–2927.
196. Xu, Y.; Chen, P.; Zhang, J.; Xie, S.; Wan, F.; Deng, J.; Cheng, X.; Hu, Y.; Liao, M.; Wang, B.; Sun, X.; Peng, H. A One-Dimensional Fluidic Nanogenerator with a High Power Conversion Efficiency. *Angew. Chem. Int. Ed.* **2017,** *56,* 12940–12945.